Editors' Suggestion

Study of $B_c(1P)^+$ states in the $B_c^+\gamma$ mass spectrum

R. Aaij *et al.*[*]
(LHCb Collaboration)

(Received 9 July 2025; accepted 30 September 2025; published 3 December 2025)

The study of a wide peaking structure in the $B_c^+\gamma$ mass spectrum is reported using a data sample of proton-proton collisions collected by the LHCb detector at center-of-mass energies of 7, 8, and 13 TeV, corresponding to an integrated luminosity of 9 fb^{-1}. The observed structure is consistent with the lowest excited P-wave B_c^+ states and exhibits a statistical significance exceeding 7 standard deviations relative to the background-only hypothesis. A two-peak model serves as an effective description of the data, with various theory-constrained models further explored to provide physical interpretation. Based on the predictions for the $B_c(1P)^+$ spectrum, the relative production cross section of the overall $B_c(1P)^+$ states with respect to the B_c^+ ground state with the transverse momentum p_{T} and rapidity y of B_c^+ mesons in the regions $p_{\mathrm{T}} < 20$ GeV/c and $2.0 < y < 4.5$ at $\sqrt{s} = 13$ TeV is measured to be $0.20 \pm 0.03 \pm 0.02 \pm 0.03$, where the uncertainty terms represent statistical, systematic, and uncertainties related to the choice of theoretical models, respectively. The results provide a test of theoretical models and deepen our understanding of quantum chromodynamics.

DOI: 10.1103/1d49-q8h4

I. INTRODUCTION

The B_c^+ meson family, composed uniquely of two different heavy quarks, serves as a distinctive probe of the nonperturbative regime of quantum chromodynamics (QCD). It is predicted to have a rich spectrum, which serves as a crucial test bed for theoretical calculations based on lattice QCD [1–4] and various other QCD-based calculations [5–27], thereby advancing our understanding of the dynamical mechanisms governing the hadronic structure.

Since the observation of the B_c^+ ground state[1] by the CDF experiment at the Tevatron collider [28,29], the investigation of the B_c^+ spectrum has long been an experimental pursuit. The excited B_c^+ states with masses below the BD threshold, which corresponds to the sum of the masses of a beauty and a charmed meson, can only decay to the ground state through radiative transitions or pion emission [9,10,30]. Therefore, the $B_c^+\gamma$ and $B_c^+\pi^+\pi^-$ systems represent the only channels to identify these low-lying excited B_c^+ states. However, these searches are inherently challenging since the B_c^+ mesons are beyond the reach of currently operating e^+e^- collider facilities, and their production in hadron collisions requires simultaneous $c\bar{c}$ and $b\bar{b}$ pair production and is therefore relatively small [10,31]. The operation of the LHC at unprecedented center-of-mass energies and high luminosity has revolutionized studies of the B_c^+ mesons. The second S-wave excited state, $B_c(2S)^+$, was first reported by the ATLAS experiment as a wide structure in the $B_c^+\pi^+\pi^-$ mass spectrum [32], which was later resolved into two narrow peaks corresponding to the $B_c(2^1S_0)^+$ and $B_c(2^3S_1)^+$ states[2] by the CMS and LHCb experiments [33,34]. To probe the $B_c(1P)^+$ states, a study of the $B_c^+\gamma$ mass spectrum is necessary. The LHCb experiment is uniquely positioned for that purpose, as evidenced by several measurements of the mass, lifetime, production and decay modes of the B_c^+ states, summarized in Ref. [35], and successful experience with the radiative decays of quarkonia [36–40].

The combination between the total spin ($S = 0$ or 1) of the $\bar{b}c$ system and the orbital angular momentum ($L = 1$) between the two quarks gives rise to four $B_c(1P)^+$ states: the spin singlet 1^1P_1 and the spin triplet 1^3P_0, 1^3P_1, and 1^3P_2. The 1^1P_1 state decays to the $B_c^+\gamma$ final state, while the spin triplet states decay to $B_c(1^3S_1)^+$ (denoted as B_c^{*+} hereafter), which subsequently decays to the $B_c^+\gamma$ final state [9,10,30]. The photon originating from the B_c^{*+} decay is expected to carry such a small energy that it escapes detection [41,42], and the reconstructed $B_c^+\gamma$ mass distribution of the $B_c(1P)^+$ states shows a peaking structure

[*]Full author list given at the end of the article.

[1]Charge conjugation is implied throughout the paper.

[2]Here applies the spectroscopic notation, $n^{2S+1}L_J$, where n gives the radial quantum number, S the sum of the quark spins, L the orbital angular momentum of the quarks, and J the total angular momentum.

TABLE I. Predicted masses for the $1P$ B_c^+ states and the mass difference $\delta M = M(B_c^{*+}) - M(B_c^+)$ between the two first S-wave states (in units of MeV$/c^2$), along with the mixing angle θ.

	δM	$M(1^3P_0)$	$M(1P_1)$	$M(1P_1')$	$M(1^3P_2)$	θ [°]
Lattice QCD [1]	41	6727	6743	6765	6783	33.4
GKLT [5]	64	6683	6717	6729	6743	17.1
GJ [6]	61	6689	6738	6757	6773	25.6
FUII [7]	55	6701	6737	6760	6772	28.5
EFG [8]	62	6699	6734	6749	6762	20.4
GI [9]	67	6706	6741	6750	6768	22.4
EQ [10]	54	6693	6731	6739	6759	18.7
LLLLGZ [11]	55	6714	6757	6776	6787	35.5
WWLC [12]	55	6705	6739	6748	6762	32.2
LTFWP [13]	53	6712	6770	6761	6783	−24.3
LLWL [14]	67	6701	6745	6754	6773	35.2
HZ [15]	63	6707	6751	6786	6802	55.0

shifted to lower values, where the shift is determined by the mass difference δM between the B_c^{*+} and B_c^+ states. Furthermore, the 1^1P_1 and 1^3P_1 states mix into the physical states $1P_1'$ and $1P_1$ according to

$$\begin{pmatrix} 1P_1' \\ 1P_1 \end{pmatrix} = \begin{pmatrix} \cos\theta & \sin\theta \\ -\sin\theta & \cos\theta \end{pmatrix} \begin{pmatrix} 1^1P_1 \\ 1^3P_1 \end{pmatrix}, \tag{1}$$

with θ the mixing angle. Due to mixing, both physical states $1P_1'$ and $1P_1$ decay to the $B_c^+\gamma$ and $B_c^{*+}\gamma$ final states. Their masses, as well as those of the 1^3P_0 and 1^3P_2 states, are calculated in Refs. [1,5–15] using lattice QCD and numerous theory approaches, with these selected predictions summarized in Table I. The most precise B_c^+ mass predictions within the framework of lattice QCD have been provided by a recent study [4], albeit for a subset of the $B_c(1P)^+$ states. In total, six peaks from $B_c(1P)^+$ states are expected in the $B_c^+\gamma$ mass spectrum: Two correspond to the masses of the $1P_1$ and $1P_1'$ states, while the remaining four are displaced by δM from the masses of the 1^3P_0, $1P_1$, $1P_1'$, and 1^3P_2 states. The differences between the reconstructed $B_c(1P)^+$ masses in the $B_c^+\gamma$ mass spectrum and the ground-state B_c^+ mass, denoted as $M(B_c^+\gamma) - M(B_c^+)$, are expected to be in the range $[340, 520]$ MeV$/c^2$ [1,5–15].

Using proton-proton (pp) collision data recorded by the LHCb experiment at center-of-mass energies of $\sqrt{s} = 7$, 8, and 13 TeV, corresponding to integrated luminosities of 1, 2, and 6 fb^{-1}, respectively, a wide peaking structure consistent with the $B_c(1P)^+$ states is observed in the $B_c^+\gamma$ system reconstructed through the $B_c^+ \to J/\psi(\to \mu^+\mu^-)\pi^+$ decay chain, as reported in Ref. [43]. This paper focuses on the interpretation of the $B_c(1P)^+$ structure and its production measurement and provides details of the selection criteria and the photon energy correction method. A brief introduction to the LHCb detector along with the reconstruction and simulation procedures is provided in Sec. II. The event selection criteria are detailed in Sec. III. The correction of the photon energy is discussed in Sec. IV. The $B_c(1P)^+$ signal yield and corresponding peak locations are determined in Sec. V using a theory-independent approach. Tests of theoretical models and measurement of $B_c(1P)^+$ production are reported in Sec. VI. Systematic uncertainties on the production rates are evaluated in Sec. VII. All results are summarized in Sec. VIII.

II. DETECTOR AND SIMULATION

The LHCb detector [44,45] is a single-arm forward spectrometer covering the pseudorapidity range $2 < \eta < 5$, designed for the study of particles containing b or c quarks. The detector includes a high-precision tracking system consisting of a silicon-strip vertex detector surrounding the pp interaction region, a large-area silicon-strip detector located upstream of a dipole magnet with a bending power of about 4 T m, and three stations of silicon-strip detectors and straw drift tubes placed downstream of the magnet. The tracking system provides a measurement of the momentum, p, of charged particles with a relative uncertainty that varies from 0.5% at low momentum to 1.0% at 200 GeV$/c$. The minimum distance of a track to a primary pp collision vertex (PV), the impact parameter (IP), is measured with a resolution of $(15 + 29/p_{\mathrm{T}})$ μm, where p_{T} is the component of the momentum transverse to the beam, in GeV$/c$. Particle identification (PID) for charged hadrons uses information from two ring-imaging Cherenkov detectors. Muons are identified by a system composed of alternating layers of iron and multiwire proportional chambers.

A calorimeter system consisting of scintillating-pad (SPD) and preshower detectors, an electromagnetic calorimeter (ECAL) and a hadronic calorimeter is responsible for the identification of photons, electrons and hadrons. The ECAL employs the Shashlik technology, i.e., a sampling scintillator/lead structure read out by plastic wavelength shifting fibers, with a design energy resolution of $\sigma_E/E = 10\%/\sqrt{E} \oplus 1\%$, with E in GeV [46]. The

ECAL energy scale is calibrated using photons from π^0 decays, as detailed in Refs. [47,48]. Photons are reconstructed from the energy deposits in the ECAL that are not associated with any reconstructed tracks [49]. For offline calibration purposes, they are separated into two categories based on their response in the SPD detector: those that have converted in the material following the dipole magnet (converted photons), thus leaving hits in the SPD, and those that have not undergone conversion (nonconverted photons) and so do not interact with the SPD. Photons that convert before the magnet can be reconstructed as a e^+e^- pair. They have excellent energy resolution given the accurate tracking information available [38,39]. However, the reconstruction efficiency is very low, and therefore, they are not used in this analysis.

The online event selection is performed by a trigger, which consists of a hardware stage based on information from the calorimeter and muon systems, followed by a software stage, which performs a full event reconstruction. The trigger selection algorithms are primarily based on identifying the key characteristics of beauty and charm hadrons to ensure maximum efficiency across the full spectrum of their possible decays. This includes considering the topological signature of their displaced vertices and imposing kinematic requirements such as on the transverse momentum of final-state particles. At the hardware stage, events are required to have at least one muon with high transverse momentum or a hadron with high transverse energy. At the software stage, two muon tracks or three charged tracks are required to have high p_T and to form a secondary vertex with a significant displacement from the interaction point.

Simulation is required to model the signal, as well as to study the effects of detector acceptance, resolution, and the selection requirements. The BcVegPy generator [50] is employed to simulate the production of $B_c(1P)^+$ and B_c^+ mesons. It is based on full perturbative QCD calculations at the lowest order (α_s^4) via the dominant gluon-gluon fusion process, while neglecting contributions from the quark-pair annihilation [51–55]. The generator is interfaced with the Pythia parton shower and hadronization model [56] with a specific LHCb configuration [57]. The decays of unstable particles are modeled using EvtGen [58], and final-state radiation is generated using Photos [59]. The interaction of the generated particles with the detector, and its response, are implemented using the Geant4 toolkit [60] as described in Ref. [61]. The simulated sample is also corrected to match the track reconstruction performance [62] and PID response [63] in data. The detector response used for particle identification is sampled from the $D^{*+} \to D^0(\to K^-\pi^+)\pi^+$ and $K_S^0 \to \pi^+\pi^-$ control channels for pions, and the $J/\psi \to \mu^+\mu^-$ control channel for muons, respectively [64]. The difference of the photon reconstruction efficiency between data and simulation is corrected using the relative yields of reconstructed $B^+ \to J/\psi K^{*+}(\to K^+\pi^0(\to \gamma\gamma))$ and $B^+ \to J/\psi K^+$ decays [65]. The energy response to photons in simulation is corrected using large calibration samples of $\chi_{c1} \to J/\psi\gamma$ decays, with converted and nonconverted photons treated separately, as described in Sec IV.

III. CANDIDATE RECONSTRUCTION AND SELECTION

The search for $B_c(1P)^+$ states is performed in the decay chain $B_c(1P)^+ \to B_c^+\gamma$, with $B_c^+ \to J/\psi\pi^+$ and $J/\psi \to \mu^+\mu^-$. The selection procedure of $B_c^+ \to J/\psi\pi^+$ candidates follows that used in Refs. [66,67] as described below. Candidate J/ψ mesons are formed by combining pairs of oppositely charged muons, each required to have $p_T > 550$ MeV/c, that originate from a common vertex. The J/ψ candidates must have a mass within the range $[3040, 3140]$ MeV/c^2, which corresponds to approximately six times the J/ψ mass resolution, and are then combined with a charged pion to form the B_c^+ candidates. The pion must satisfy $p_T > 1000$ MeV/c and be inconsistent with originating from any PV. The B_c^+ candidates are required to have a good-quality vertex fit, a decay time exceeding 0.2 ps, and a momentum vector aligned with the displacement vector identified by the decay vertex and the associated PV. The latter represents the vertex with the smallest impact parameter $\chi^2_{\rm IP}$, defined as the difference in the vertex-fit χ^2 of a given PV with and without the B_c^+ candidate.

To further suppress combinatorial background, a boosted decision tree (BDT) [68,69] classifier is applied. The input variables comprise the transverse momentum p_T of the muons, the pion, and the J/ψ meson; the decay length, decay time, and vertex-fit χ^2 of the B_c^+ meson, as well as the $\chi^2_{\rm IP}$ values of the muons, the pion, the J/ψ meson, and the B_c^+ meson relative to the associated PV. The classifier is trained on simulated signal candidates and background candidates from the upper sideband of the $J/\psi\pi^+$ mass spectrum in data, within the mass range $[6370, 6600]$ MeV/c^2. The BDT selection working point is optimized to maximize the figure of merit $S/\sqrt{S+B}$, where S and B denote the expected signal and background yields, respectively, in the mass window $M(J/\psi\pi^+) \in [6251, 6301]$ MeV/c^2, which corresponds to approximately four times the B_c^+ mass resolution.

To form the $B_c(1P)^+$ candidates, the selected B_c^+ candidates within the mass range $[6240, 6300]$ MeV/c^2 are combined with photons detected by the calorimeter system. The majority of photons originate from the decay of neutral pions, i.e., $\pi^0 \to \gamma\gamma$. This background contribution is reduced by discarding photons with a companion photon such that the diphoton mass is within a ± 30 MeV/c^2 region from the known π^0 mass [70]. Further photon selections are implemented to maximize the Punzi figure of merit [71], $S/(5/2 + \sqrt{B})$, for $B_c(1P)^+$ signals in the expected mass region. These enforce that

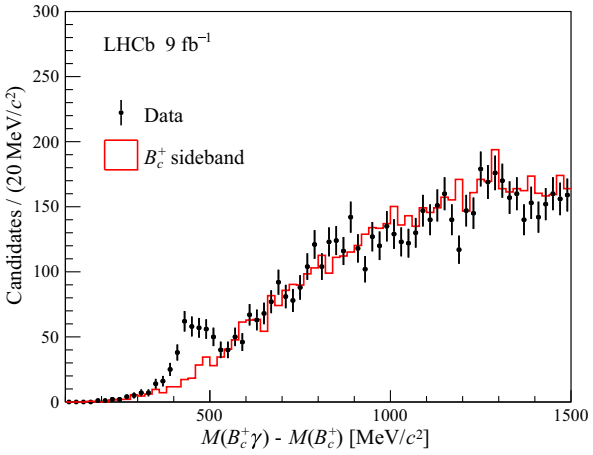

FIG. 1. Distribution of $M(B_c^+\gamma) - M(B_c^+)$ for the selected B_c^+ candidates. The distribution of B_c^+ candidates from the high-mass sideband region is also shown for comparison.

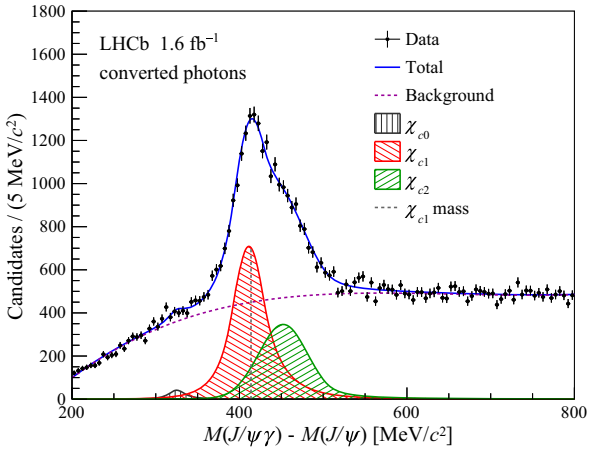

FIG. 2. Distribution of $M(J/\psi\gamma) - M(J/\psi)$ for selected χ_c candidates with converted photons, in the region $E_\gamma \in [5.9, 7.2]$ GeV and $n_{\text{tracks}} \in [125, 181]$. Fit results are also shown. Contributions from χ_{c0},χ_{c1}, and χ_{c2} decays are shown with different line colors, while the gray vertical line indicates the known χ_{c1} mass [70].

photons have transverse energy $E_{\text{T}} > 1000$ MeV, $E > 4000$ MeV, and a high probability of being correctly identified, based on the value of a neural-net estimator that combines information from the calorimeter and tracking systems [72]. Finally, to reduce background contributions from multiple photon combinations with the same B_c^+ meson, only the candidate with the highest E_{T} photon is kept.

The distribution of $M(B_c^+\gamma) - M(B_c^+)$ for selected B_c^+ candidates is shown in Fig. 1, This variable is chosen to minimize effects from the B_c^+ mass resolution. The corresponding distribution, obtained by considering B_c^+ candidates from the high-mass sideband region ($M(B_c^+) \in [6340, 6550]$ MeV/c^2), is also shown for comparison. It demonstrates that the chosen selection criteria do not introduce artificial peaks in the pure background sample. A pronounced peaking structure is evident within the predicted mass range of the $B_c(1P)^+$ states.

IV. PHOTON ENERGY CORRECTION IN SIMULATION

To determine the signal composition of the peaking structure, a good understanding of the photon energy scale and resolution is required. Dedicated corrections are applied to the simulation to accurately model the location and width of the signal peaks. These corrections are obtained using large data and simulated samples of $\chi_c \to J/\psi\gamma$ decays, where the photon energy spectrum is similar to that in the signal decays. The selection criteria applied to photons are identical to those used for the $B_c(1P)^+$ candidates, which ensures portability of the corrections.

Photon energy corrections in simulation are derived from fits to the $J/\psi\gamma$ mass distributions in data. They are obtained separately for converted and nonconverted photons in each data taking period, and in two-dimensional regions of the photon energy, E_γ, and the number of reconstructed tracks, n_{tracks}. An example of the $M(J/\psi\gamma) - M(J/\psi)$ distribution of converted photons in one typical E_γ and n_{tracks} region using 2016 data is shown in Fig. 2. The distribution shows a wide peaking structure due to the contributions from the χ_{c0}, χ_{c1}, and χ_{c2} states. These resonant contributions are each modeled as a nonrelativistic Breit–Wigner function convolved with a modified Gaussian function with asymmetric power-law tails to account for the mass resolution. The natural widths of the χ_c states are fixed to their known values [70]. The background component is modeled by a third-order polynomial function. In each E_γ and n_{tracks} region, the photon energy bias and resolution are determined based on their linear relationship with two observables: the deviation of the χ_{c1} peak location from its known value [70] and the measured width of the χ_{c1} mass peak. The linear dependencies are well established by simulation studies.

The simulated samples of $B_c(1P)^+ \to B_c^+\gamma$ are generated with different $B_c(1P)^+$ masses within the theoretical prediction range. The signal shape in $M(B_c^+\gamma) - M(B_c^+)$ distribution is corrected on a per-candidate basis, using the photon energy bias and resolution of the corresponding E_γ and n_{tracks} region. With the corrections applied, the $B_c^+\gamma$ signal resolution is parametrized as a modified Gaussian function with asymmetric power-law tails. The resolution, σ, and peak location, μ, are found to have a small linear dependency on the true mass difference of the $B_c(1P)^+$ signal peak in simulation, ΔM_{true}, given by $\mu = -0.006 \times \Delta M_{\text{true}} - 0.340$ MeV/c^2 and $\sigma = 0.041 \times \Delta M_{\text{true}} + 1.640$ MeV/c^2. These dependencies are used to fully constrain the signal shape for a given mass hypothesis.

A self-consistency check of the photon energy correction is performed by applying the same method to the $\chi_{c1} \to J/\psi\gamma$ and $\chi_{c2} \to J/\psi\gamma$ decays. A good agreement between the corrected mass and the value in data is obtained, and the measured mass resolution is well reproduced. As an example, using samples with converted photons from the 2016 data-taking period, the difference between the χ_{c1} mass determined from the simulation and the data is reduced from 2.0 MeV/c^2 to 0.3 MeV/c^2, and the difference in resolution decreases from 0.3 MeV/c^2 to 0.1 MeV/c^2, due to the application of the photon energy correction. Similarly, for the χ_{c2} state, the difference in mass is reduced from 2.0 MeV/c^2 to 0.4 MeV/c^2 and the resolution improves from 0.7 MeV/c^2 to 0.4 MeV/c^2.

Another channel, $D_{s1}(2460)^+ \to D_s^+\gamma$, is used to independently validate the correction method and assess the associated systematic uncertainty. The $D_{s1}(2460)^+$ channel has a similar photon energy spectrum and decay topology to the signal channel. The same photon selection criteria as for the $B_c(1P)^+$ candidates are applied. The $M(D_s^+\gamma) - M(D_s^+)$ distribution for converted photons in 2016 data is shown in Fig. 3 as an example, along with the result of a fit. The signal model for $D_{s1}(2460)^+$ is a Gaussian function with asymmetric power-law tails, while the background model is an exponential function. The peak location and resolution in data are consistently reproduced by the corrected simulation. Across all the data subsets, the largest difference remaining in the $D_{s1}(2460)^+$ mass between data and simulation is 2.9 MeV/c^2, compared to 3.6 MeV/c^2 before the correction, while the difference in resolution decreases from 4.6 MeV/c^2 to 2.6 MeV/c^2. The residual difference in the $D_{s1}(2460)^+$ mass is scaled to the signal channel $B_c(1P)^+ \to B_c^+\gamma$ according to the energy released in the decays and taken as the systematic uncertainty arising from the photon energy correction for the $B_c(1P)^+$ mass measurement.

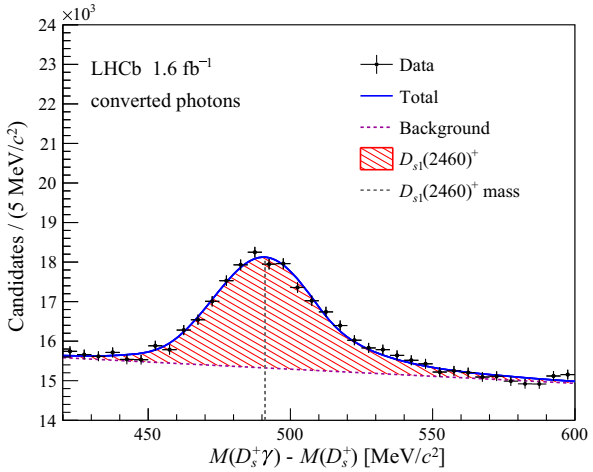

FIG. 3. Distribution of $M(D_s^+\gamma) - M(D_s^+)$ for the selected $D_{s1}(2460)^+$ candidates with converted photons. Fit results are also shown. The gray vertical line indicates the known $D_{s1}(2460)^+$ mass [70].

V. THEORY-INDEPENDENT MASS FIT

As displayed in Fig. 1, a peaking structure is clearly visible in the $M(B_c^+\gamma) - M(B_c^+)$ distribution. It exhibits a significance above 7 standard deviations when compared to the background-only hypothesis, taking into account the look-elsewhere effect within the predicted mass region [73], as detailed in Ref. [43]. The root mean square of the structure is approximately 62 MeV/c^2, which largely exceeds the expected value of about 36 MeV/c^2 for a single peak based on the corrected simulation, thus indicating the presence of multiple overlapping states. An unbinned extended maximum-likelihood fit, independent of theoretical inputs, is performed using a minimal two-peak model to describe the observed structure, as detailed in Ref. [43]. The natural widths of the $B_c(1P)^+$ states are expected to be only a few hundred keV [5,74] and are neglected due to their small effect compared to the resolution. Each peak is modeled by a modified Gaussian function with asymmetric power-law tails as determined from Sec. IV, leaving only the peak location free to vary in the fit. The combinatorial background is described by a monotonically increasing third-order polynomial function [75]. The locations of the two peaks are measured to be

$$M_1 = 6704.8 \pm 5.5 \pm 2.8 \pm 0.3 \text{ MeV}/c^2,$$
$$M_2 = 6752.4 \pm 9.5 \pm 3.1 \pm 0.3 \text{ MeV}/c^2,$$

where the uncertainties are statistical, systematic, and from the limited knowledge on the B_c^+ mass, given as 6274.5 ± 0.3 MeV/c^2 [70]. The statistical correlation between the two measured peak locations is +56%, while their systematic uncertainties are fully correlated.

VI. $B_c(1P)^+$ PRODUCTION

Given the current experimental resolution, the two-peak hypothesis serves as the minimal model that effectively describes the data, and extracting more information from the data alone is challenging. Therefore, a theory-constrained model consisting of six peaks is proposed to further explore the properties of the unresolved $B_c(1P)^+$ states. In this framework, the positions of all six peaks are constrained to the theoretical predictions of $M(B_c(1P)^+) - M(B_c^+)$, whereas those arising from decays with an unreconstructed soft photon from the intermediate B_c^{*+} state are shifted by δM accordingly. Their resolutions are determined from the linear dependence derived from simulations generated at different $B_c(1P)^+$ masses. The production cross section of the $B_c(1P)^+$ states relative to the B_c^+ ground state, denoted as R, is measured in the fiducial region $p_T(B_c^+) < 20$ GeV/c and $2.0 < y(B_c^+) < 4.5$, where y is

the rapidity, at the center-of-mass energy of $\sqrt{s} = 13$ TeV, using data corresponding to an integrated luminosity of 6 fb^{-1}. This subsample is considered to facilitate a direct comparison with theoretical predictions from NRQCD-based calculations [10,31,50,76–79] at this center-of-mass energy. The relative production rate is measured as

$$R = \frac{N(B_c(1P)^+ \to B_c^+\gamma)}{N(B_c^+)} \cdot \frac{\varepsilon(B_c^+)}{\varepsilon(B_c(1P)^+ \to B_c^+\gamma)}, \quad (2)$$

where $N(B_c(1P)^+ \to B_c^+\gamma)$ and $N(B_c^+)$ are the signals yields determined from fits to the mass spectra. The terms $\varepsilon(B_c^+)$ and $\varepsilon(B_c(1P)^+ \to B_c^+\gamma)$ are the corresponding total detection efficiencies for inclusive $B_c^+ \to J/\psi\pi^+$ and $B_c(1P)^+ \to B_c^+\gamma$, respectively, determined using simulation. With the six $B_c(1P)^+$ peaks predicted from the theory-constrained model, the detection efficiencies $\varepsilon(B_c(1P)^+ \to B_c^+\gamma)$ are evaluated separately for each corresponding decay process, with or without the intermediate B_c^{*+} state.

Figure 4 shows the mass distribution of the B_c^+ candidates, with the dimuon mass constrained to the known mass of the J/ψ meson [70] and the B_c^+ candidates required to originate from the associated PV [80]. An unbinned extended maximum-likelihood fit is performed on the mass distribution of the selected B_c^+ candidates to extract the B_c^+ signal yield. In the fit, both the signal and the background component due to Cabibbo-suppressed decays $B_c^+ \to J/\psi K^+$, where the kaon is misidentified as a pion, are modeled using a modified Gaussian function with asymmetric power-law tails. The model parameters are fixed from simulation except for the peak location and width of the signal, which are free in the fit, and the peak location of the $B_c^+ \to J/\psi K^+$ background, which is constrained relative to that of the signal. The combinatorial background is described with an exponential function.

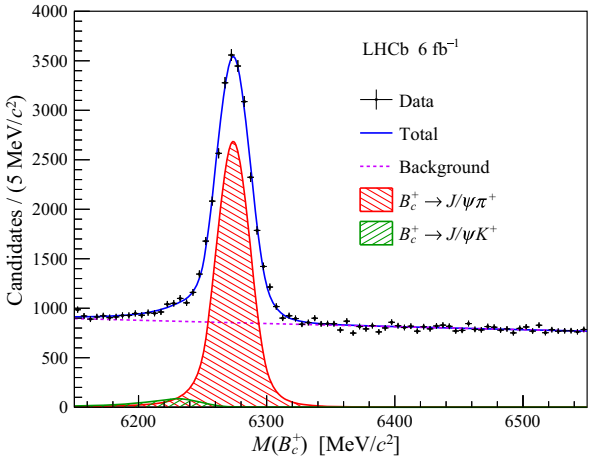

FIG. 4. Mass distribution of the selected B_c^+ candidates reconstructed from the $B_c^+ \to J/\psi\pi^+$ decay. The fit results are also shown.

TABLE II. Production cross sections for $B_c(1P)^+$ and $B_c(2S)^+$ states (in unit of nb) calculated using the latest BcVegPy 2.2 setup [50] for pp collisions at $\sqrt{s} = 13$ TeV, in the kinematic region defined by $p_T(B_c^+) < 20$ GeV/c and $2.0 < y(B_c^+) < 4.5$.

	1^1P_1	1^3P_0	1^3P_1	1^3P_2	2^1S_0	2^3S_1
σ_{prod} [nb]	3.5	1.1	2.7	7.2	4.5	11.1

The signal yield of the selected B_c^+ candidates is determined to be $(18.70 \pm 0.21) \times 10^3$.

In the theory-constrained fit to the $B_c^+\gamma$ candidates, the overall $B_c(1P)^+$ signal shape is defined using theoretical inputs. A rich set of theoretical predictions on the $B_c(1P)^+$ mass spectrum is taken into account, as listed in Table I. These predictions are used to fix the location of each peak, while the resolution is determined by the mass-resolution relation described in Sec. IV. In addition, the relative yields of the six signal components are also fixed to stabilize the fit. The contribution from the ith signal component is given by

$$N_i = \mathcal{L} \cdot \sigma_{\text{prod},i} \cdot \mathcal{B}_i \cdot \varepsilon_i, \quad (3)$$

where $\mathcal{L}$ represents the integrated luminosity and is common to all components, $\sigma_{\text{prod},i}$ is the production cross section, $\mathcal{B}_i$ is the decay branching ratio, and ε_i is the detection efficiency. The branching ratios $\mathcal{B}_i$ for the $1P_1$ and $1P_1'$ states decaying to $B_c^+\gamma$ or $B_c^{*+}\gamma$ are calculated based on Ref. [9], with the masses and the mixing angle replaced by the values taken from each theoretical model. The inclusive production cross sections for each of the four $B_c(1P)^+$ states include both direct production, as reported in Table II, and feed-down contributions from the decays of

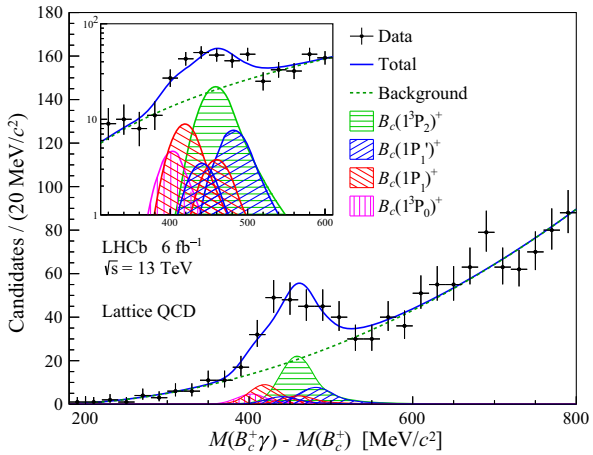

FIG. 5. Distribution of the mass difference $M(B_c^+\gamma) - M(B_c^+)$ with the result of the lattice QCD fit model also shown. The contributions of the six signal peaks from four $B_c(1P)^+$ states are shown, where both the location and the relative contributions are fixed to the central values predicted by C.T.H. Davies *et al.* [1]. The inset illustrates a zoomed signal region in logarithmic scale.

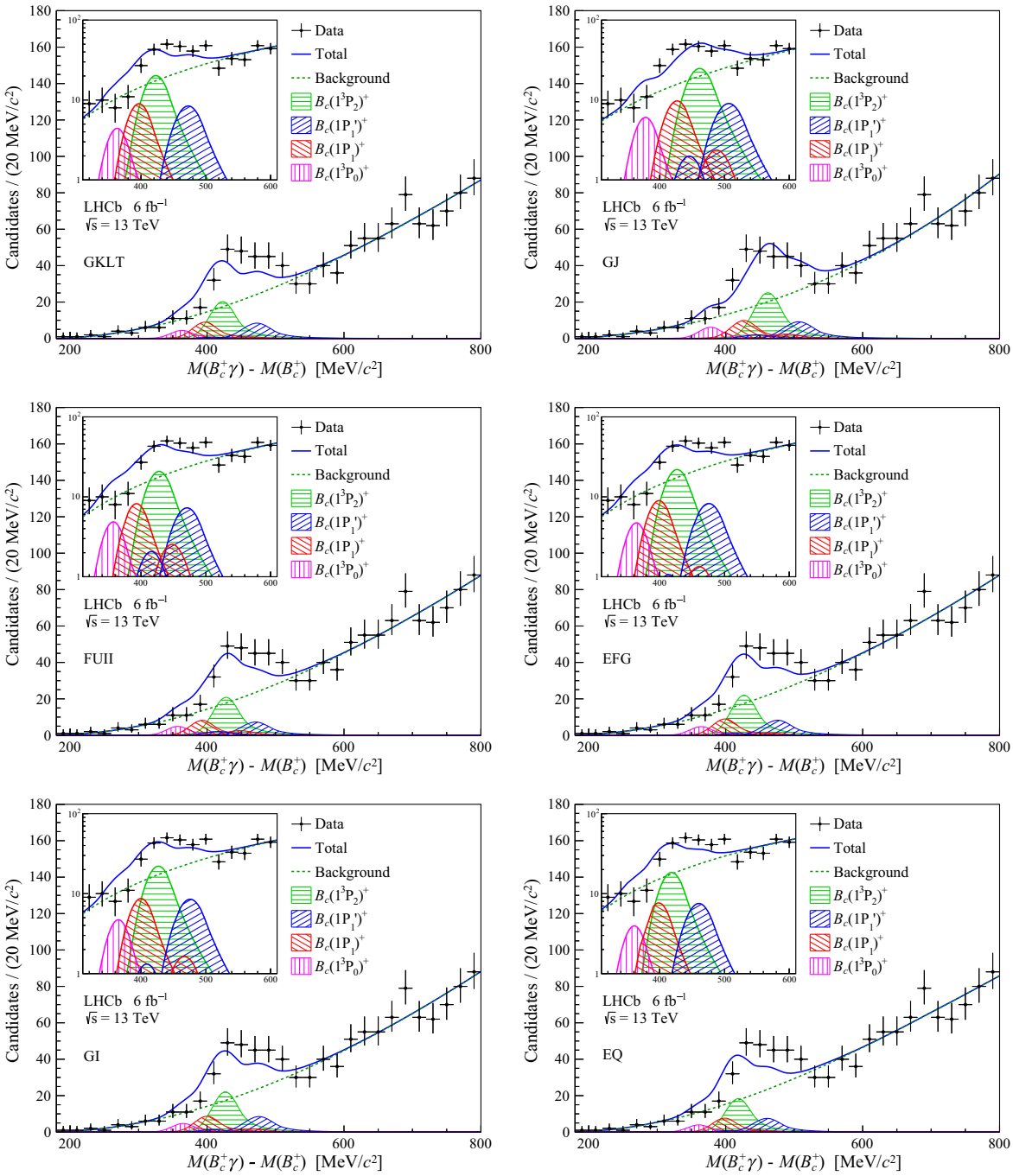

FIG. 6. The caption for each plot is the same as Fig. 5. Both the location and the relative contributions are fixed to the central value predicted by (top left) GKLT [5]; (top right) GJ [6]; (middle left) FUII [7]; (middle right) EFG [8]; (bottom left) GI [9]; (bottom right) EQ [10].

excited $B_c(2S)^+$ states. The branching fractions for these feed-down processes are calculated according to Ref. [9]. The detection efficiency is evaluated using fully simulated samples generated with BcVegPy where the kinematic distributions are corrected to match the various decay modes of the $B_c(1P)^+$ states. With the peak locations and relative contributions of each component fixed, the overall $B_c(1P)^+$ signal shape is obtained for each theoretical model, allowing the summed $B_c(1P)^+$ signal yield to be determined from the fit.

An unbinned extended maximum-likelihood fit to the $M(B_c^+\gamma) - M(B_c^+)$ distribution is performed for each theoretical model, where the background component is modeled by a third-order polynomial function monotonically increasing in the fit range. All the considered models provide a generally good description of the data,

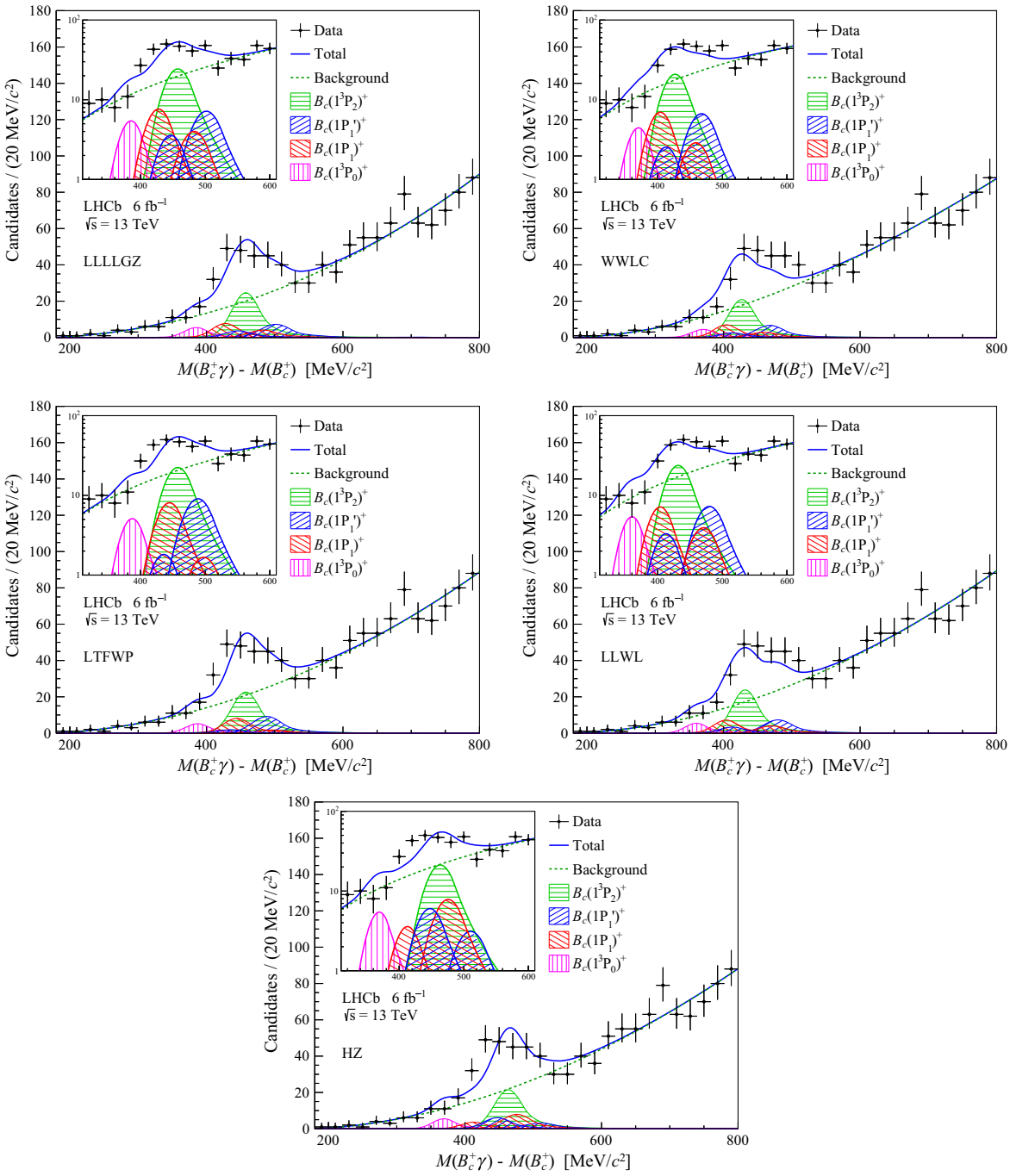

FIG. 7. The caption for each plot is the same as Fig. 5. Both the location and the relative contributions are fixed to the central value predicted by (top left) LLLLGZ [11]; (top right) WWLC [12]; (middle left) LTFWP [13]; (middle right) LLWL [14]; (bottom) HZ [15].

with p values ranging from 15% to 90%, as estimated using the Kolmogorov–Smirnov criterion [81]. The fit results are shown in Figs. 5–7. The fit quality of a given model depends not only on the predicted masses but also on the relative yields of the six signal components. These yields are governed by the predicted production cross sections [50] and branching fractions [9], the latter of which additionally incorporate the mixing angle as an input parameter.

The fit shown in Fig. 5 is selected as the baseline for the production measurement as it provides the best p value. It is based on the lattice QCD calculations of Ref. [1]. The signal yield of $B_c(1P)^+$ is determined to be 153 ± 22, including only the statistical uncertainty. It is further corrected for a tiny (1.3%) contribution from misidentified $B_c^+ \to J/\psi K^+$ candidates. The theoretical uncertainty is evaluated as the largest difference between the baseline result and those obtained from alternative QCD models that

are consistent with the data within one standard deviation [6–9,11–15]. The largest deviation is assigned as the theoretical model uncertainty. The relative production rate is measured to be

$$R = 0.20 \pm 0.03 \pm 0.03,$$

where the terms denote statistical and theoretical uncertainties, respectively. The result is consistent with NRQCD-based theoretical predictions [9,10]. These predictions, calculated with BcVegPy, yield values from 0.17 to 0.19, including color-octet contributions and feed-down from $B_c(2S)^+$ decays.

VII. SYSTEMATIC UNCERTAINTIES ON PRODUCTION MEASUREMENT

Several sources of systematic uncertainty that affect the measurement of the relative production rate are considered. Their contributions are summarized in Table III and treated as uncorrelated. The imperfect modeling of the signal and background shapes can affect the $B_c(1P)^+$ and B_c^+ yields, biasing the final result. Therefore, alternative fit models are used to assess their potential impact. The signal shapes of B_c^+ and each $B_c(1P)^+$ components are replaced with a sum of the original modified Gaussian function with asymmetric power-law tails and an additional Gaussian function, leading to a systematic uncertainty of 0.8%. For the B_c^+ background shape, the exponential function is replaced with a second-order polynomial function, while the background for $B_c(1P)^+$ is described using a monotonically increasing fourth-order polynomial function instead. The difference with respect to the nominal result is 6.9%, taken as the corresponding systematic uncertainty.

In the efficiency calculation, the photon detection efficiency is corrected using results from Ref. [65]. The correction factors are determined from the relative yields of $B^+ \to J/\psi K^{*+}(\to K^+\pi^0)$ versus $B^+ \to J/\psi K^+$ events. The uncertainty in the correction factors, primarily due to the branching ratio of $B^+ \to J/\psi K^{*+}$ [70], is propagated through the efficiency evaluation and included as a systematic uncertainty of 3.5% in the final results. The systematic uncertainty due to the limited size of the simulated samples is well below 1%. The imperfect simulation of particle identification, track reconstruction, and trigger largely cancels in the relative production rate. Their impact is estimated to be of 1% each. The systematic uncertainties are in addition to the contribution of 14% due to the choice of the theoretical model, which is accounted for separately.

TABLE III. Summary of relative systematic uncertainties on the measurement of the production rate between $B_c(1P)^+$ and B_c^+ states. The total uncertainty is calculated as the sum in quadrature of individual contributions.

Source	$\delta R/R$ [%]
Background shape	6.9
Signal shape	0.8
Photon detection	3.5
Simulation sample size	0.6
Track reconstruction	1.0
PID requirement	1.0
Trigger requirement	1.0
Total	8.0

VIII. CONCLUSION

In summary, using pp collision data corresponding to an integrated luminosity of 9 fb^{-1} collected by the LHCb experiment at center-of-mass energies of 7, 8, and 13 TeV, a wide peaking structure is observed in the $B_c^+\gamma$ mass spectrum with a significance larger than seven standard deviations. The structure is compatible with the lowest P-wave excited states of the beauty-charm meson, as verified by fits based on the theoretical predictions from lattice QCD [1] and various QCD models [5–15]. The structure is well described by a minimal two-peak model in a theory-independent approach, with their measured masses reported in Ref. [43]. The distinction between contributions from each $B_c(1P)^+$ state requires larger statistics and significant improvements in mass resolution, potentially achieved by using photons that convert in the detector material and are reconstructed as e^+e^- pairs [38,39], which may enable a measurement of the B_c^{*+} and B_c^+ mass difference. Such a measurement is of significant theoretical interest and would be challenging to perform otherwise.

Using a subset of data collected at $\sqrt{s} = 13$ TeV, the fraction of B_c^+ mesons from $B_c(1P)^+$ decays is measured in the B_c^+ kinematic region $p_T < 20\ \text{GeV}/c$ and $2.0 < y < 4.5$. It is determined to be

$$R = 0.20 \pm 0.03 \pm 0.02 \pm 0.03,$$

where the first, second, and third uncertainties are statistical, systematic, and theoretical, respectively. The measured value is in good agreement with expectations from NRQCD-based calculations. These results represent the first observation of orbitally excited beauty-charm states and measurement of their production properties, providing crucial insights into the internal dynamics of hadrons containing two heavy quarks and the nonperturbative aspects of QCD.

ACKNOWLEDGMENTS

We thank Xing-Gang Wu for valuable discussions on the B_c^+ production issues. We express our gratitude to our colleagues in the CERN accelerator departments for the excellent performance of the LHC. We thank the technical and administrative staff at the LHCb institutes. We

acknowledge support from CERN and from the national agencies: ARC (Australia); CAPES, CNPq, FAPERJ and FINEP (Brazil); MOST and NSFC (China); CNRS/IN2P3 (France); BMBF, DFG and MPG (Germany); INFN (Italy); NWO (Netherlands); MNiSW and NCN (Poland); MCID/IFA (Romania); MICIU and AEI (Spain); SNSF and SER (Switzerland); NASU (Ukraine); STFC (United Kingdom); DOE NP and NSF (USA). We acknowledge the computing resources that are provided by ARDC (Australia), CBPF (Brazil), CERN, IHEP and LZU (China), IN2P3 (France), KIT and DESY (Germany), INFN (Italy), SURF (Netherlands), Polish WLCG (Poland), IFIN-HH (Romania), PIC (Spain), CSCS (Switzerland), and GridPP (United Kingdom). We are indebted to the communities behind the multiple open-source software packages on which we depend. Individual groups or members have received support from Key Research Program of Frontier Sciences of CAS, CAS PIFI, CAS CCEPP, Fundamental Research Funds for the Central Universities, and Sci. & Tech. Program of Guangzhou (China); Minciencias (Colombia); EPLANET, Marie Skłodowska-Curie Actions, ERC and NextGenerationEU (European Union); A*MIDEX, ANR, IPhU and Labex P2IO, and Région Auvergne-Rhône-Alpes (France); Alexander-von-Humboldt Foundation (Germany); ICSC (Italy); Severo Ochoa and María de Maeztu Units of Excellence, GVA, XuntaGal, GENCAT, InTalent-Inditex and Prog. Atracción Talento CM (Spain); SRC (Sweden); the Leverhulme Trust, the Royal Society and UKRI (United Kingdom).

DATA AVAILABILITY

The data that support the findings of this article are openly available [82].

[1] C. T. H. Davies, K. Hornbostel, G. P. Lepage, A. J. Lidsey, J. Shigemitsu, , and J. Sloan, B_c spectroscopy from lattice QCD, Phys. Lett. B **382**, 131 (1996).
[2] H. P. Shanahan, P. Boyle, C. T. H. Davies, and H. Newton (UKQCD Collaboration), A nonperturbative calculation of the mass of the B_c, Phys. Lett. B **453**, 289 (1999).
[3] I. F. Allison, C. T. H. Davies, A. Gray, A. S. Kronfeld, P. B. Mackenzie, and J. N. Simone (HPQCD Collaboration, Fermilab Lattice Collaboration, and UKQCD Collaboration), Mass of the B_c meson in three-flavor lattice QCD, Phys. Rev. Lett. **94**, 172001 (2005).
[4] N. Mathur, M. Padmanath, and S. Mondal, Precise predictions of charmed-bottom hadrons from lattice QCD, Phys. Rev. Lett. **121**, 202002 (2018).
[5] S. S. Gershtein, V. V. Kiselev, A. K. Likhoded, and A. V. Tkabladze, B_c spectroscopy, Phys. Rev. D **51**, 3613 (1995).
[6] S. N. Gupta and J. M. Johnson, B_c spectroscopy in a quantum-chromodynamic potential model, Phys. Rev. D **53**, 312 (1996).
[7] L. P. Fulcher, Phenomenological predictions of the properties of the B_c system, Phys. Rev. D **60**, 074006 (1999).
[8] D. Ebert, R. N. Faustov, and V. O. Galkin, Properties of heavy quarkonia and B_c mesons in the relativistic quark model, Phys. Rev. D **67**, 014027 (2003).
[9] S. Godfrey, Spectroscopy of B_c mesons in the relativized quark model, Phys. Rev. D **70**, 054017 (2004).
[10] E. J. Eichten and C. Quigg, Mesons with beauty and charm: new horizons in spectroscopy, Phys. Rev. D **99**, 054025 (2019).
[11] Q. Li, M.-S. Liu, L.-S. Lu, Q.-F. Lü, L.-C. Gui, and X.-H. Zhong, Excited bottom-charmed mesons in a nonrelativistic quark model, Phys. Rev. D **99**, 096020 (2019).
[12] G.-L. Wang, T. Wang, Q. Li, and C.-H. Chang, The mass spectrum and wave functions of the B_c system, J. High Energy Phys. 05 (2022) 006.
[13] T.-Y. Li, L. Tang, Z.-Y. Fang, C.-H. Wang, C.-Q. Pang, Higher states of the B_c meson family, Phys. Rev. D **108**, 034019 (2023).
[14] X.-J. Li, Y.-S. Li, F.-L. Wang, and X. Liu, Spectroscopic survey of higher-lying states of B_c meson family, Eur. Phys. J. C **83**, 1080 (2023).
[15] W. Hao and R. Zhu, Beauty-charm meson family with coupled channel effects and their strong decays, Chin. Phys. C **48**, 123101 (2024).
[16] Y.-Q. Chen and Y.-P. Kuang, Improved QCD-motivated heavy quark potentials with explicit $\Lambda_{\overline{\mathrm{MS}}}$ dependence, Phys. Rev. D **46**, 1165 (1992); **47**, 350(E) (1993).
[17] J. Zeng, J. W. Van Orden, and W. Roberts, Heavy mesons in a relativistic model, Phys. Rev. D **52**, 5229 (1995).
[18] A. Abd El-Hady, J. R. Spence, and J. P. Vary, Radiative decays of B_c mesons in a Bethe–Salpeter model, Phys. Rev. D **71**, 034006 (2005).
[19] K.-W. Wei and X.-H. Guo, Mass spectra of doubly heavy mesons in Regge phenomenology, Phys. Rev. D **81**, 076005 (2010).
[20] R. J. Dowdall, C. T. H. Davies, T. C. Hammant, and R. R. Horgan, Precise heavy-light meson masses and hyperfine splittings from lattice QCD including charm quarks in the sea, Phys. Rev. D **86**, 094510 (2012).
[21] Z.-G. Wang, Analysis of the vector and axialvector B_c mesons with QCD sum rules, Eur. Phys. J. A **49**, 131 (2013).
[22] M. Karliner and J. L. Rosner, Scaling of P-wave excitation energies in heavy-quark systems, Phys. Rev. D **98**, 074026 (2018).
[23] M. Chen, L. Chang, and Y.-X. Liu, B_c meson spectrum via Dyson–Schwinger equation and Bethe–Salpeter equation approach, Phys. Rev. D **101**, 056002 (2020).
[24] B. Martín-González, P. G. Ortega, D. R. Entem, F. Fernández, and J. Segovia, Toward the discovery of novel

B_c states: Radiative and hadronic transitions, Phys. Rev. D **106**, 054009 (2022).
[25] S. Nussinov, Mass inequalities in QCD, Phys. Rev. Lett. **52**, 966 (1984).
[26] R. A. Bertlmann and A. Martin, Inequalities on heavy quark-antiquark systems, Nucl. Phys. **B168**, 111 (1980).
[27] N. R. Soni, B. R. Joshi, R. P. Shah, H. R. Chauhan, and J. N. Pandya, $Q\bar{Q}$ ($Q \in \{b, c\}$) spectroscopy using the Cornell potential, Eur. Phys. J. C **78**, 592 (2018).
[28] F. Abe *et al.* (CDF Collaboration), Observation of the B_c meson in $p\bar{p}$ collisions at $\sqrt{s} = 1.8$ TeV, Phys. Rev. Lett. **81**, 2432 (1998).
[29] F. Abe *et al.* (CDF Collaboration), Observation of B_c mesons in $p\bar{p}$ collisions at $\sqrt{s} = 1.8$ TeV, Phys. Rev. D **58**, 112004 (1998).
[30] I. P. Gouz, V. V. Kiselev, A. K. Likhoded, V. I. Romanovsky, and O. P. Yushchenko, Prospects for the B_c studies at LHCb, Phys. At. Nucl. **67**, 1559 (2004).
[31] C.-H. Chang, C.-F. Qiao, J.-X. Wang, and X.-G. Wu, Color-octet contributions to P-wave B_c meson hadroproduction, Phys. Rev. D **71**, 074012 (2005).
[32] G. Aad *et al.* (ATLAS Collaboration), Observation of an excited $B_c^{\pm}$ meson state with the ATLAS detector, Phys. Rev. Lett. **113**, 212004 (2014).
[33] A. M. Sirunyan *et al.* (CMS Collaboration), Observation of two excited B_c^+ states and measurement of the $B_c^+(2S)$ mass in pp collisions at $\sqrt{s} = 13$ TeV, Phys. Rev. Lett. **122**, 132001 (2019).
[34] R. Aaij *et al.* (LHCb Collaboration), Observation of an excited B_c^+ state, Phys. Rev. Lett. **122**, 232001 (2019).
[35] R. Aaij *et al.* (LHCb Collaboration), Observation of the $B_c^+ \to J/\psi\pi^+\pi^0$ decay, J. High Energy Phys. 04 (2024) 151.
[36] R. Aaij *et al.* (LHCb Collaboration), Measurement of the cross section ratio $\sigma(\chi_{c2})/\sigma(\chi_{c1})$ for prompt χ_c production at $\sqrt{s} = 7$ TeV, Phys. Lett. B **714**, 215 (2012).
[37] R. Aaij *et al.* (LHCb Collaboration), Measurement of the ratio of prompt χ_c to J/ψ production in p p collisions at $\sqrt{s} = 7$ TeV, Phys. Lett. B **718**, 431 (2012).
[38] R. Aaij *et al.* (LHCb Collaboration), Measurement of the relative rate of prompt χ_{c0}, χ_{c1} and χ_{c2} production at $\sqrt{s} = 7$ TeV, J. High Energy Phys. 10 (2013) 115.
[39] R. Aaij *et al.* (LHCb Collaboration), Measurement of the $\chi_b(3P)$ mass and of the relative rate of $\chi_{b1}(1P)$ and $\chi_{b2}(1P)$ production, J. High Energy Phys. 10 (2014) 088.
[40] R. Aaij *et al.* (LHCb Collaboration), Study of χ_b meson production in p p collisions at $\sqrt{s} = 7$ and 8 TeV and observation of the decay $\chi_b \to \Upsilon(3S)\gamma$, Eur. Phys. J. C **74**, 3092 (2014).
[41] A. Berezhnoy and A. Likhoded, The observation possibility of B_c excitations at LHC, Proc. Sci. QFTHEP2013 (**2013**) 051 [arXiv:1307.5993].
[42] A. V. Berezhnoy, I. N. Belov, A. K. Likhoded, and A. V. Luhinsky, B_c excitations at LHC experiments, Mod. Phys. Lett. A **34**, 1950331 (2019).
[43] R. Aaij *et al.* (LHCb collaboration), companion paper, Observation of orbitally excited B_c^+ states, Phys. Rev. Lett. **135**, 231902 (2025).
[44] A. A. Alves Jr. *et al.* (LHCb Collaboration), The LHCb detector at the LHC, J. Instrum. **3**, S08005 (2008).
[45] R. Aaij *et al.* (LHCb Collaboration), LHCb detector performance, Int. J. Mod. Phys. A **30**, 1530022 (2015).
[46] LHCb Collaboration, LHCb calorimeters, CERN, Technical design report, CERN-LHCC-2000-036, 2000.
[47] I. M. Belyaev, D. Y. Golubkov, V. Y. Egorychev, and D. V. Savrina, Calibration of the LHCb electromagnetic calorimeter using the technique of neutral pion invariant mass reconstruction, Instrum. Exp. Tech. **57**, 33 (2014).
[48] C. Abellán Beteta *et al.*, Calibration and performance of the LHCb calorimeters in Run 1 and 2 at the LHC, arXiv: 2008.11556.
[49] O. Deschamps *et al.*, Photon and neutral pion reconstruction, CERN, LHCb-2003-091, 2003.
[50] C.-H. Chang, X.-Y. Wang, and X.-G. Wu, BcVegPy2.2: A newly upgraded version for hadronic production of the meson B_c^+ and its excited states, Comput. Phys. Commun. **197**, 335 (2015).
[51] C.-H. Chang and Y.-Q. Chen, The hadronic production of the B_c meson at Tevatron, LHC and SSC, Phys. Rev. D **48**, 4086 (1993).
[52] C.-H. Chang, Y.-Q. Chen, G.-P. Han, and H.-T. Jiang, On hadronic production of the B_c meson, Phys. Lett. B **364**, 78 (1995).
[53] C.-H. Chang, Y.-Q. Chen, and R. J. Oakes, Comparative study of the hadronic production of B_c mesons, Phys. Rev. D **54**, 4344 (1996).
[54] C.-H. Chang, J.-X. Wang, and X.-G. Wu, Hadronic production of the P-wave excited B_c-states $B_{cJ}^*(L = 1)$, Phys. Rev. D **70**, 114019 (2004).
[55] A. V. Berezhnoy, V. V. Kiselev, and A. K. Likhoded, Hadronic production of S- and P-wave states of $\bar{b}c$ quarkonium, Z. Phys. A **356**, 79 (1996).
[56] T. Sjöstrand, S. Mrenna, and P. Skands, A brief introduction to PYTHIA 8.1, Comput. Phys. Commun. **178**, 852 (2008).
[57] I. Belyaev *et al.*, Handling of the generation of primary events in Gauss, the LHCb simulation framework, J. Phys. Conf. Ser. **331**, 032047 (2011).
[58] D. J. Lange, The EvtGen particle decay simulation package, Nucl. Instrum. Methods Phys. Res., Sect. A **462**, 152 (2001).
[59] N. Davidson, T. Przedzinski, and Z. Was, PHOTOS interface in C++: Technical and physics documentation, Comput. Phys. Commun. **199**, 86 (2016).
[60] J. Allison *et al.* (Geant4 Collaboration), Geant4 developments and applications, IEEE Trans. Nucl. Sci. **53** (2006) 270; S. Agostinelli *et al.* (Geant4 Collaboration), Geant4: A simulation toolkit, Nucl. Instrum. Methods Phys. Res., Sect. A **506**, 250 (2003).
[61] M. Clemencic, G. Corti, S. Easo, C. R. Jones, S. Miglioranzi, M. Pappagallo, and P. Robbe, The LHCb simulation application, Gauss: Design, evolution and experience, J. Phys. Conf. Ser. **331**, 032023 (2011).
[62] R. Aaij *et al.* (LHCb Collaboration), Measurement of the track reconstruction efficiency at LHCb, J. Instrum. **10**, P02007 (2015).
[63] F. Archilli *et al.*, Performance of the muon identification at LHCb, J. Instrum. **8**, P10020 (2013).
[64] R. Aaij *et al.*, Selection and processing of calibration samples to measure the particle identification performance

of the LHCb experiment in Run 2, Eur. Phys. J. Tech. Instrum. **6**, 1 (2019).
[65] E. Govorkova, Study of π^0/γ efficiency using B meson decays in the LHCb experiment, Phys. At. Nucl. **79**, 1474 (2016).
[66] R. Aaij *et al.* (LHCb Collaboration), Precision measurement of the B_c^+ meson mass, J. High Energy Phys. 07 (2020) 123.
[67] R. Aaij *et al.* (LHCb Collaboration), Observation of an excited B_c^+ state, Phys. Rev. Lett. **122**, 232001 (2019).
[68] L. Breiman, J. H. Friedman, R. A. Olshen, and C. J. Stone, *Classification and Regression Trees* (Wadsworth International Group, Belmont, CA, 1984).
[69] Y. Freund and R. E. Schapire, A decision-theoretic generalization of on-line learning and an application to boosting, J. Comput. Syst. Sci. **55**, 119 (1997).
[70] S. Navas *et al.* (Particle Data Group), Review of particle physics, Phys. Rev. D **110**, 030001 (2024).
[71] G. Punzi, Sensitivity of searches for new signals and its optimization, eConf **C030908**, MODT002 (2003).
[72] M. Hoballah, Measurement of the photon polarization using $B_s^0 \to \phi\gamma$ at LHCb., Ph.D. thesis, CERN-THESIS-2015-073, Clermont-Ferrand Unuversity, 2015.
[73] E. Gross and O. Vitells, Trial factors for the look elsewhere effect in high energy physics, Eur. Phys. J. C **70**, 525 (2010).
[74] E. J. Eichten and C. Quigg, Mesons with beauty and charm: Spectroscopy, Phys. Rev. D **49**, 5845 (1994).
[75] S. Karlin and L. S. Shapley, *Geometry of Moment Spaces* (American Mathematical Society, Providence, 1953), Vol. 12.
[76] C.-H. Chang, C. Driouichi, P. Eerola, and X. G. Wu, BcVegPy An event generator for hadronic production of the B_c meson, Comput. Phys. Commun. **159**, 192 (2004).
[77] C.-H. Chang, J.-X. Wang, and X.-G. Wu, BcVegPy2.0: An upgrade version of the generator BcVegPy with an addendum about hadroproduction of the P-wave B_c states, Comput. Phys. Commun. **174**, 241 (2006).
[78] X.-Y. Wang and X.-G. Wu, A trick to improve the efficiency of generating unweighted B_c events from BcVegPy, Comput. Phys. Commun. **183**, 442 (2012).
[79] X.-G. Wu, BcVegPy and GenXicc for the hadronic production of the doubly heavy mesons and baryons, J. Phys. Conf. Ser. **523**, 012042 (2014).
[80] W. D. Hulsbergen, Decay chain fitting with a Kalman filter, Nucl. Instrum. Methods Phys. Res., Sect. A **552**, 566 (2005).
[81] N. V. Smirnov, On the estimation of the discrepancy between empirical curves of distribution for two independent samples, Bull. Math. Univ. Moscou **2**, 3 (1939).
[82] https://cds.cern.ch/record/2937507.

R. Aaij,[38] A. S. W. Abdelmotteleb,[57] C. Abellan Beteta,[51] F. Abudinén,[57] T. Ackernley,[61] A. A. Adefisoye,[69] B. Adeva,[47] M. Adinolfi,[55] P. Adlarson,[84] C. Agapopoulou,[14] C. A. Aidala,[86] Z. Ajaltouni,[11] S. Akar,[11] K. Akiba,[38] P. Albicocco,[28] J. Albrecht,[19,b] F. Alessio,[49] Z. Aliouche,[63] P. Alvarez Cartelle,[56] R. Amalric,[16] S. Amato,[3] J. L. Amey,[55] Y. Amhis,[14] L. An,[6] L. Anderlini,[27] M. Andersson,[51] P. Andreola,[51] M. Andreotti,[26] S. Andres Estrada,[83] A. Anelli,[31,49,c] D. Ao,[7] F. Archilli,[37,d] Z Areg,[69] M. Argenton,[26] S. Arguedas Cuendis,[9,49] A. Artamonov,[44] M. Artuso,[69] E. Aslanides,[13] R. Ataíde Da Silva,[50] M. Atzeni,[65] B. Audurier,[12] J. A. Authier,[15] D. Bacher,[64] I. Bachiller Perea,[50] S. Bachmann,[22] M. Bachmayer,[50] J. J. Back,[57] P. Baladron Rodriguez,[47] V. Balagura,[15] A. Balboni,[26] W. Baldini,[26] L. Balzani,[19] H. Bao,[7] J. Baptista de Souza Leite,[61] C. Barbero Pretel,[47,12] M. Barbetti,[27] I. R. Barbosa,[70] R. J. Barlow,[63] M. Barnyakov,[25] S. Barsuk,[14] W. Barter,[59] J. Bartz,[69] S. Bashir,[40] B. Batsukh,[5] P. B. Battista,[14] A. Bay,[50] A. Beck,[65] M. Becker,[19] F. Bedeschi,[35] I. B. Bediaga,[2] N. A. Behling,[19] S. Belin,[47] K. Belous,[44] I. Belov,[29] I. Belyaev,[36] G. Benane,[13] G. Bencivenni,[28] E. Ben-Haim,[16] A. Berezhnoy,[44] R. Bernet,[51] S. Bernet Andres,[46] A. Bertolin,[33] C. Betancourt,[51] F. Betti,[59] J. Bex,[56] Ia. Bezshyiko,[51] O. Bezshyyko,[85] J. Bhom,[41] M. S. Bieker,[18] N. V. Biesuz,[26] P. Billoir,[16] A. Biolchini,[38] M. Birch,[62] F. C. R. Bishop,[10] A. Bitadze,[63] A. Bizzeti,[27,e] T. Blake,[57,f] F. Blanc,[50] J. E. Blank,[19] S. Blusk,[69] V. Bocharnikov,[44] J. A. Boelhauve,[19] O. Boente Garcia,[15] T. Boettcher,[68] A. Bohare,[59] A. Boldyrev,[44] C. S. Bolognani,[81] R. Bolzonella,[26,g] R. B. Bonacci,[1] N. Bondar,[44,49] A. Bordelius,[49] F. Borgato,[33,49] S. Borghi,[63] M. Borsato,[31,c] J. T. Borsuk,[82] E. Bottalico,[61] S. A. Bouchiba,[50] M. Bovill,[64] T. J. V. Bowcock,[61] A. Boyer,[49] C. Bozzi,[26] J. D. Brandenburg,[87] A. Brea Rodriguez,[50] N. Breer,[19] J. Brodzicka,[41] A. Brossa Gonzalo,[47,a] J. Brown,[61] D. Brundu,[32] E. Buchanan,[59] L. Buonincontri,[33,h] M. Burgos Marcos,[81] A. T. Burke,[63] C. Burr,[49] J. S. Butter,[56] J. Buytaert,[49] W. Byczynski,[49] S. Cadeddu,[32] H. Cai,[74] Y. Cai,[5] A. Caillet,[16] R. Calabrese,[26,g] S. Calderon Ramirez,[9] L. Calefice,[45] S. Cali,[28] M. Calvi,[31,c] M. Calvo Gomez,[46] P. Camargo Magalhaes,[2,i] J. I. Cambon Bouzas,[47] P. Campana,[28] D. H. Campora Perez,[81] A. F. Campoverde Quezada,[7] S. Capelli,[31] L. Capriotti,[26] R. Caravaca-Mora,[9] A. Carbone,[25,j] L. Carcedo Salgado,[47] R. Cardinale,[29,k] A. Cardini,[32] P. Carniti,[31] L. Carus,[22] A. Casais Vidal,[65] R. Caspary,[22] G. Casse,[61] M. Cattaneo,[49] G. Cavallero,[26] V. Cavallini,[26,g]

S. Celani,[22] S. Cesare,[30,l] A. J. Chadwick,[61] I. Chahrour,[86] H. Chang,[4,m] M. Charles,[16] Ph. Charpentier,[49] E. Chatzianagnostou,[38] R. Cheaib,[78] M. Chefdeville,[10] C. Chen,[56] J. Chen,[50] S. Chen,[5] Z. Chen,[7] M. Cherif,[12] A. Chernov,[41] S. Chernyshenko,[53] X. Chiotopoulos,[81] V. Chobanova,[83] M. Chrzaszcz,[41] A. Chubykin,[44] V. Chulikov,[28,36] P. Ciambrone,[28] X. Cid Vidal,[47] G. Ciezarek,[49] P. Cifra,[38] P. E. L. Clarke,[59] M. Clemencic,[49] H. V. Cliff,[56] J. Closier,[49] C. Cocha Toapaxi,[22] V. Coco,[49] J. Cogan,[13] E. Cogneras,[11] L. Cojocariu,[43] S. Collaviti,[50] P. Collins,[49] T. Colombo,[49] M. Colonna,[19] A. Comerma-Montells,[45] L. Congedo,[24] J. Connaughton,[57] A. Contu,[32] N. Cooke,[60] C. Coronel,[66] I. Corredoira,[12] A. Correia,[16] G. Corti,[49] J. Cottee Meldrum,[55] B. Couturier,[49] D. C. Craik,[51] M. Cruz Torres,[2,n] E. Curras Rivera,[50] R. Currie,[59] C. L. Da Silva,[68] S. Dadabaev,[44] L. Dai,[71] X. Dai,[4] E. Dall'Occo,[49] J. Dalseno,[83] C. D'Ambrosio,[62] J. Daniel,[11] P. d'Argent,[24] G. Darze,[3] A. Davidson,[57] J. E. Davies,[63] O. De Aguiar Francisco,[63] C. De Angelis,[32,o] F. De Benedetti,[49] J. de Boer,[38] K. De Bruyn,[80] S. De Capua,[63] M. De Cian,[63] U. De Freitas Carneiro Da Graca,[2,p] E. De Lucia,[28] J. M. De Miranda,[2] L. De Paula,[3] M. De Serio,[24,q] P. De Simone,[28] F. De Vellis,[19] J. A. de Vries,[81] F. Debernardis,[24] D. Decamp,[10] S. Dekkers,[1] L. Del Buono,[16] B. Delaney,[65] H.-P. Dembinski,[19] J. Deng,[8] V. Denysenko,[51] O. Deschamps,[11] F. Dettori,[32,o] B. Dey,[78] P. Di Nezza,[28] I. Diachkov,[44] S. Didenko,[44] S. Ding,[69] Y. Ding,[50] L. Dittmann,[22] V. Dobishuk,[53] A. D. Docheva,[60] A. Doheny,[57] C. Dong,[4,m] A. M. Donohoe,[23] F. Dordei,[32] A. C. dos Reis,[2] A. D. Dowling,[69] L. Dreyfus,[13] W. Duan,[72] P. Duda,[82] M. W. Dudek,[41] L. Dufour,[49] V. Duk,[34] P. Durante,[49] M. M. Duras,[82] J. M. Durham,[68] O. D. Durmus,[78] A. Dziurda,[41] A. Dzyuba,[44] S. Easo,[58] E. Eckstein,[18] U. Egede,[1] A. Egorychev,[44] V. Egorychev,[44] S. Eisenhardt,[59] E. Ejopu,[63] L. Eklund,[84] M. Elashri,[66] J. Ellbracht,[19] S. Ely,[62] A. Ene,[43] J. Eschle,[69] S. Esen,[22] T. Evans,[38] F. Fabiano,[32] S. Faghih,[66] L. N. Falcao,[2] B. Fang,[7] R. Fantechi,[35] L. Fantini,[34,r] M. Faria,[50] K. Farmer,[59] D. Fazzini,[31,c] L. Felkowski,[82] M. Feng,[5,7] M. Feo,[19] A. Fernandez Casani,[48] M. Fernandez Gomez,[47] A. D. Fernez,[67] F. Ferrari,[25,j] F. Ferreira Rodrigues,[3] M. Ferrillo,[51] M. Ferro-Luzzi,[49] S. Filippov,[44] R. A. Fini,[24] M. Fiorini,[26,g] M. Firlej,[40] K. L. Fischer,[64] D. S. Fitzgerald,[86] C. Fitzpatrick,[63] T. Fiutowski,[40] F. Fleuret,[15] A. Fomin,[52] M. Fontana,[25] L. F. Foreman,[63] R. Forty,[49] D. Foulds-Holt,[59] V. Franco Lima,[3] M. Franco Sevilla,[67] M. Frank,[49] E. Franzoso,[26,g] G. Frau,[63] C. Frei,[49] D. A. Friday,[63] J. Fu,[7] Q. Führing,[19,56,b] T. Fulghesu,[13] G. Galati,[24] M. D. Galati,[38] A. Gallas Torreira,[47] D. Galli,[25,j] S. Gambetta,[59] M. Gandelman,[3] P. Gandini,[30] B. Ganie,[63] H. Gao,[7] R. Gao,[64] T. Q. Gao,[56] Y. Gao,[8] Y. Gao,[6] Y. Gao,[8] L. M. Garcia Martin,[50] P. Garcia Moreno,[45] J. García Pardiñas,[65] P. Gardner,[67] K. G. Garg,[8] L. Garrido,[45] C. Gaspar,[49] A. Gavrikov,[33] L. L. Gerken,[19] E. Gersabeck,[20] M. Gersabeck,[20] T. Gershon,[57] S. Ghizzo,[29,k] Z. Ghorbanimoghaddam,[55] L. Giambastiani,[33,h] F. I. Giasemis,[16,s] V. Gibson,[56] H. K. Giemza,[42] A. L. Gilman,[64] M. Giovannetti,[28] A. Gioventù,[45] L. Girardey,[63,58] M. A. Giza,[41] F. C. Glaser,[14,22] V. V. Gligorov,[16] C. Göbel,[70] L. Golinka-Bezshyyko,[85] E. Golobardes,[46] D. Golubkov,[44] A. Golutvin,[62,49] S. Gomez Fernandez,[45] W. Gomulka,[40] I. Gonçales Vaz,[49] F. Goncalves Abrantes,[64] M. Goncerz,[41] G. Gong,[4,m] J. A. Gooding,[19] I. V. Gorelov,[44] C. Gotti,[31] E. Govorkova,[65] J. P. Grabowski,[18] L. A. Granado Cardoso,[49] E. Graugés,[45] E. Graverini,[50,t] L. Grazette,[57] G. Graziani,[27] A. T. Grecu,[43] L. M. Greeven,[38] N. A. Grieser,[66] L. Grillo,[60] S. Gromov,[44] C. Gu,[15] M. Guarise,[26] L. Guerry,[11] V. Guliaeva,[44] P. A. Günther,[22] A.-K. Guseinov,[50] E. Gushchin,[44] Y. Guz,[6,49] T. Gys,[49] K. Habermann,[18] T. Hadavizadeh,[1] C. Hadjivasiliou,[67] G. Haefeli,[50] C. Haen,[49] G. Hallett,[57] P. M. Hamilton,[67] J. Hammerich,[61] Q. Han,[33] X. Han,[22,49] S. Hansmann-Menzemer,[22] L. Hao,[7] N. Harnew,[64] T. H. Harris,[1] M. Hartmann,[14] S. Hashmi,[40] J. He,[7,u] F. Hemmer,[49] C. Henderson,[66] R. Henderson,[14] R. D. L. Henderson,[1] A. M. Hennequin,[49] K. Hennessy,[61] L. Henry,[50] J. Herd,[62] P. Herrero Gascon,[22] J. Heuel,[17] A. Hicheur,[3] G. Hijano Mendizabal,[51] J. Horswill,[63] R. Hou,[8] Y. Hou,[11] D. C. Houston,[60] N. Howarth,[61] J. Hu,[72] W. Hu,[7] X. Hu,[4,m] W. Hulsbergen,[38] R. J. Hunter,[57] M. Hushchyn,[44] D. Hutchcroft,[61] M. Idzik,[40] D. Ilin,[44] P. Ilten,[66] A. Iniukhin,[44] A. Ishteev,[44] K. Ivshin,[44] H. Jage,[17] S. J. Jaimes Elles,[76,49,48] S. Jakobsen,[49] E. Jans,[38] B. K. Jashal,[48] A. Jawahery,[67] C. Jayaweera,[54] V. Jevtic,[19] Z. Jia,[16] E. Jiang,[67] X. Jiang,[5,7] Y. Jiang,[7] Y. J. Jiang,[6] N. Jindal,[87] M. John,[64] A. John Rubesh Rajan,[23] D. Johnson,[54] C. R. Jones,[56] T. P. Jones,[57] S. Joshi,[42] B. Jost,[49] J. Juan Castella,[56] N. Jurik,[49] I. Juszczak,[41] D. Kaminaris,[50] S. Kandybei,[52] M. Kane,[59] Y. Kang,[4,m] C. Kar,[11] M. Karacson,[49] A. Kauniskangas,[50] J. W. Kautz,[66] M. K. Kazanecki,[41] F. Keizer,[49] M. Kenzie,[56] T. Ketel,[38] B. Khanji,[69] A. Kharisova,[44] S. Kholodenko,[35,49] G. Khreich,[14] T. Kirn,[17]

V. S. Kirsebom,[31,c] O. Kitouni,[65] S. Klaver,[39] N. Kleijne,[35,v] K. Klimaszewski,[42] M. R. Kmiec,[42] S. Koliiev,[53] L. Kolk,[19] A. Konoplyannikov,[6] P. Kopciewicz,[49] P. Koppenburg,[38] A. Korchin,[52] M. Korolev,[44] I. Kostiuk,[38] O. Kot,[53] S. Kotriakhova, E. Kowalczyk,[67] A. Kozachuk,[44] P. Kravchenko,[44] L. Kravchuk,[44] M. Kreps,[57] P. Krokovny,[44] W. Krupa,[69] W. Krzemien,[42] O. Kshyvanskyi,[53] S. Kubis,[82] M. Kucharczyk,[41] V. Kudryavtsev,[44] E. Kulikova,[44] A. Kupsc,[84] V. Kushnir,[52] B. Kutsenko,[13] I. Kyryllin,[52] D. Lacarrere,[49] P. Laguarta Gonzalez,[45] A. Lai,[32] A. Lampis,[32] D. Lancierini,[62] C. Landesa Gomez,[47] J. J. Lane,[1] G. Lanfranchi,[28] C. Langenbruch,[22] J. Langer,[19] O. Lantwin,[44] T. Latham,[57] F. Lazzari,[35,49,t] C. Lazzeroni,[54] R. Le Gac,[13] H. Lee,[61] R. Lefèvre,[11] A. Leflat,[44] S. Legotin,[44] M. Lehuraux,[57] E. Lemos Cid,[49] O. Leroy,[13] T. Lesiak,[41] E. D. Lesser,[49] B. Leverington,[22] A. Li,[4,m] C. Li,[4] C. Li,[13] H. Li,[72] J. Li,[8] K. Li,[75] L. Li,[63] M. Li,[8] P. Li,[7] P.-R. Li,[73] Q. Li,[5,7] S. Li,[8] T. Li,[71] T. Li,[72] Y. Li,[8] Y. Li,[5] Y. Li,[4] Z. Lian,[4,m] Q. Liang,[8] X. Liang,[69] S. Libralon,[48] C. Lin,[7] T. Lin,[58] R. Lindner,[49] H. Linton,[62] R. Litvinov,[32] D. Liu,[8] F. L. Liu,[1] G. Liu,[72] K. Liu,[73] S. Liu,[5,7] W. Liu,[8] Y. Liu,[59] Y. Liu,[73] Y. L. Liu,[62] G. Loachamin Ordonez,[70] A. Lobo Salvia,[45] A. Loi,[32] T. Long,[56] J. H. Lopes,[3] A. Lopez Huertas,[45] C. Lopez Iribarnegaray,[47] S. López Soliño,[47] Q. Lu,[15] C. Lucarelli,[49] D. Lucchesi,[33,h] M. Lucio Martinez,[48] Y. Luo,[6] A. Lupato,[33,w] E. Luppi,[26,g] K. Lynch,[23] X.-R. Lyu,[7] G. M. Ma,[4,m] S. Maccolini,[19] F. Machefert,[14] F. Maciuc,[43] B. Mack,[69] I. Mackay,[64] L. M. Mackey,[69] L. R. Madhan Mohan,[56] M. J. Madurai,[54] D. Magdalinski,[38] D. Maisuzenko,[44] J. J. Malczewski,[41] S. Malde,[64] L. Malentacca,[49] A. Malinin,[44] T. Maltsev,[44] G. Manca,[32,o] G. Mancinelli,[13] C. Mancuso,[14] R. Manera Escalero,[45] F. M. Manganella,[37] D. Manuzzi,[25] D. Marangotto,[30,l] J. F. Marchand,[10] R. Marchevski,[50] U. Marconi,[25] E. Mariani,[16] S. Mariani,[49] C. Marin Benito,[45] J. Marks,[22] A. M. Marshall,[55] L. Martel,[64] G. Martelli,[34] G. Martellotti,[36] L. Martinazzoli,[49] M. Martinelli,[31,c] D. Martinez Gomez,[80] D. Martinez Santos,[83] F. Martinez Vidal,[48] A. Martorell i Granollers,[46] A. Massafferri,[2] R. Matev,[49] A. Mathad,[49] V. Matiunin,[44] C. Matteuzzi,[69] K. R. Mattioli,[15] A. Mauri,[62] E. Maurice,[15] J. Mauricio,[45] P. Mayencourt,[50] J. Mazorra de Cos,[48] M. Mazurek,[42] M. McCann,[62] T. H. McGrath,[63] N. T. McHugh,[60] A. McNab,[63] R. McNulty,[23] B. Meadows,[66] G. Meier,[19] D. Melnychuk,[42] D. Mendoza Granada,[16] F. M. Meng,[4,m] M. Merk,[38,81] A. Merli,[50,30] L. Meyer Garcia,[67] D. Miao,[5,7] H. Miao,[7] M. Mikhasenko,[77] D. A. Milanes,[76,x] A. Minotti,[31,c] E. Minucci,[28] T. Miralles,[11] B. Mitreska,[19] D. S. Mitzel,[19] A. Modak,[58] L. Moeser,[19] R. A. Mohammed,[64] R. D. Moise,[17] E. F. Molina Cardenas,[86] T. Mombächer,[49] M. Monk,[57,1] S. Monteil,[11] A. Morcillo Gomez,[47] G. Morello,[28] M. J. Morello,[35,v] M. P. Morgenthaler,[22] J. Moron,[40] W. Morren,[38] A. B. Morris,[49] A. G. Morris,[13] R. Mountain,[69] H. Mu,[4,m] Z. M. Mu,[6] E. Muhammad,[57] F. Muheim,[59] M. Mulder,[80] K. Müller,[51] F. Muñoz-Rojas,[9] R. Murta,[62] V. Mytrochenko,[52] P. Naik,[61] T. Nakada,[50] R. Nandakumar,[58] T. Nanut,[49] I. Nasteva,[3] M. Needham,[59] E. Nekrasova,[44] N. Neri,[30,l] S. Neubert,[18] N. Neufeld,[49] P. Neustroev,[44] J. Nicolini,[49] D. Nicotra,[81] E. M. Niel,[15] N. Nikitin,[44] Q. Niu,[73] P. Nogarolli,[3] P. Nogga,[18] C. Normand,[55] J. Novoa Fernandez,[47] G. Nowak,[66] C. Nunez,[86] H. N. Nur,[60] A. Oblakowska-Mucha,[40] V. Obraztsov,[44] T. Oeser,[17] A. Okhotnikov,[44] O. Okhrimenko,[53] R. Oldeman,[32,o] F. Oliva,[59,49] E. Olivart Pino,[45] M. Olocco,[19] C. J. G. Onderwater,[81] R. H. O'Neil,[49] J. S. Ordonez Soto,[11] D. Osthues,[19] J. M. Otalora Goicochea,[3] P. Owen,[51] A. Oyanguren,[48] O. Ozcelik,[49] F. Paciolla,[35,y] A. Padee,[42] K. O. Padeken,[18] B. Pagare,[47] T. Pajero,[49] A. Palano,[24] M. Palutan,[28] C. Pan,[74] X. Pan,[4,m] S. Panebianco,[12] G. Panshin,[5] L. Paolucci,[57] A. Papanestis,[58] M. Pappagallo,[24,q] L. L. Pappalardo,[26] C. Pappenheimer,[66] C. Parkes,[63] D. Parmar,[77] B. Passalacqua,[26,g] G. Passaleva,[27] D. Passaro,[35,49,v] A. Pastore,[24] M. Patel,[62] J. Patoc,[64] C. Patrignani,[25,j] A. Paul,[69] C. J. Pawley,[81] A. Pellegrino,[38] J. Peng,[5,7] X. Peng,[73] M. Pepe Altarelli,[28] S. Perazzini,[25] D. Pereima,[44] H. Pereira Da Costa,[68] A. Pereiro Castro,[47] C. Perez,[46] P. Perret,[11] A. Perrevoort,[80] A. Perro,[49,13] M. J. Peters,[66] K. Petridis,[55] A. Petrolini,[29,k] J. P. Pfaller,[66] H. Pham,[69] L. Pica,[35,v] M. Piccini,[34] L. Piccolo,[32] B. Pietrzyk,[10] G. Pietrzyk,[14] R. N. Pilato,[61] D. Pinci,[36] F. Pisani,[49] M. Pizzichemi,[31,49,c] V. M. Placinta,[43] M. Plo Casasus,[47] T. Poeschl,[49] F. Polci,[16] M. Poli Lener,[28] A. Poluektov,[13] N. Polukhina,[44] I. Polyakov,[63] E. Polycarpo,[3] S. Ponce,[49] D. Popov,[7,49] S. Poslavskii,[44] K. Prasanth,[59] C. Prouve,[83] D. Provenzano,[32,49,o] V. Pugatch,[53] G. Punzi,[35,t] S. Qasim,[51] Q. Q. Qian,[6] W. Qian,[7] N. Qin,[4,m] S. Qu,[4,m] R. Quagliani,[49] R. I. Rabadan Trejo,[57] J. H. Rademacker,[55] M. Rama,[35] M. Ramírez García,[86] V. Ramos De Oliveira,[70] M. Ramos Pernas,[57] M. S. Rangel,[3] F. Ratnikov,[44] G. Raven,[39] M. Rebollo De Miguel,[48] F. Redi,[30,w] J. Reich,[55] F. Reiss,[20] Z. Ren,[7] P. K. Resmi,[64] M. Ribalda Galvez,[45] R. Ribatti,[50] G. Ricart,[15,12]

D. Riccardi,[35,v] S. Ricciardi,[58] K. Richardson,[65] M. Richardson-Slipper,[56] K. Rinnert,[61] P. Robbe,[14,49] G. Robertson,[60] E. Rodrigues,[61] A. Rodriguez Alvarez,[45] E. Rodriguez Fernandez,[47] J. A. Rodriguez Lopez,[76] E. Rodriguez Rodriguez,[49] J. Roensch,[19] A. Rogachev,[44] A. Rogovskiy,[58] D. L. Rolf,[19] P. Roloff,[49] V. Romanovskiy,[66] A. Romero Vidal,[47] G. Romolini,[26,49] F. Ronchetti,[50] T. Rong,[6] M. Rotondo,[28] S. R. Roy,[22] M. S. Rudolph,[69] M. Ruiz Diaz,[22] R. A. Ruiz Fernandez,[47] J. Ruiz Vidal,[81] J. J. Saavedra-Arias,[9] J. J. Saborido Silva,[47] S. E. R. Sacha Emile R.,[49] R. Sadek,[15] N. Sagidova,[44] D. Sahoo,[78] N. Sahoo,[54] B. Saitta,[32,o] M. Salomoni,[31,49,c] I. Sanderswood,[48] R. Santacesaria,[36] C. Santamarina Rios,[47] M. Santimaria,[28] L. Santoro,[2] E. Santovetti,[37] A. Saputi, D. Saranin,[44] A. Sarnatskiy,[80] G. Sarpis,[49] M. Sarpis,[79] C. Satriano,[36,z] M. Saur,[73] D. Savrina,[44] H. Sazak,[17] F. Sborzacchi,[49,28] A. Scarabotto,[19] S. Schael,[17] S. Scherl,[61] M. Schiller,[22] H. Schindler,[49] M. Schmelling,[21] B. Schmidt,[49] S. Schmitt,[17] H. Schmitz,[18] O. Schneider,[50] A. Schopper,[62] N. Schulte,[19] M. H. Schune,[14] G. Schwering,[17] B. Sciascia,[28] A. Sciuccati,[49] I. Segal,[77] S. Sellam,[47] A. Semennikov,[44] T. Senger,[51] M. Senghi Soares,[39] A. Sergi,[29,k] N. Serra,[51] L. Sestini,[27] A. Seuthe,[19] B. Sevilla Sanjuan,[46] Y. Shang,[6] D. M. Shangase,[86] M. Shapkin,[44] R. S. Sharma,[69] I. Shchemerov,[44] L. Shchutska,[50] T. Shears,[61] L. Shekhtman,[44] Z. Shen,[38] S. Sheng,[5,7] V. Shevchenko,[44] B. Shi,[7] Q. Shi,[7] W. S. Shi,[72] Y. Shimizu,[14] E. Shmanin,[25] R. Shorkin,[44] J. D. Shupperd,[69] R. Silva Coutinho,[69] G. Simi,[33,h] S. Simone,[24,q] M. Singha,[78] N. Skidmore,[57] T. Skwarnicki,[69] M. W. Slater,[54] E. Smith,[65] K. Smith,[68] M. Smith,[62] L. Soares Lavra,[59] M. D. Sokoloff,[66] F. J. P. Soler,[60] A. Solomin,[55] A. Solovev,[44] N. S. Sommerfeld,[18] R. Song,[1] Y. Song,[50] Y. Song,[4,m] Y. S. Song,[6] F. L. Souza De Almeida,[69] B. Souza De Paula,[3] E. Spadaro Norella,[29,k] E. Spedicato,[25] J. G. Speer,[19] E. Spiridenkov,[44] P. Spradlin,[60] V. Sriskaran,[49] F. Stagni,[49] M. Stahl,[77] S. Stahl,[49] S. Stanislaus,[64] M. Stefaniak,[87] E. N. Stein,[49] O. Steinkamp,[51] H. Stevens,[19] D. Strekalina,[44] Y. Su,[7] F. Suljik,[64] J. Sun,[32] J. Sun,[63] L. Sun,[74] D. Sundfeld,[2] W. Sutcliffe,[51] K. Swientek,[40] F. Swystun,[56] A. Szabelski,[42] T. Szumlak,[40] Y. Tan,[4,m] Y. Tang,[74] Y. T. Tang,[7] M. D. Tat,[22] J. A. Teijeiro Jimenez,[47] A. Terentev,[44] F. Terzuoli,[35,y] F. Teubert,[49] E. Thomas,[49] D. J. D. Thompson,[54] A. R. Thomson-Strong,[59] H. Tilquin,[62] V. Tisserand,[11] S. T'Jampens,[10] M. Tobin,[5] T. T. Todorov,[20] L. Tomassetti,[26,g] G. Tonani,[30] X. Tong,[6] T. Tork,[30] D. Torres Machado,[2] L. Toscano,[19] D. Y. Tou,[4,m] C. Trippl,[46] G. Tuci,[22] N. Tuning,[38] L. H. Uecker,[22] A. Ukleja,[40] D. J. Unverzagt,[22] A. Upadhyay,[49] B. Urbach,[59] A. Usachov,[39] A. Ustyuzhanin,[44] U. Uwer,[22] V. Vagnoni,[25] V. Valcarce Cadenas,[47] G. Valenti,[25] N. Valls Canudas,[49] J. van Eldik,[49] H. Van Hecke,[68] E. van Herwijnen,[62] C. B. Van Hulse,[47,aa] R. Van Laak,[50] M. van Veghel,[38] G. Vasquez,[51] R. Vazquez Gomez,[45] P. Vazquez Regueiro,[47] C. Vázquez Sierra,[83] S. Vecchi,[26] J. J. Velthuis,[55] M. Veltri,[27,bb] A. Venkateswaran,[50] M. Verdoglia,[32] M. Vesterinen,[57] W. Vetens,[69] D. Vico Benet,[64] P. Vidrier Villalba,[45] M. Vieites Diaz,[47] X. Vilasis-Cardona,[46] E. Vilella Figueras,[61] A. Villa,[25] P. Vincent,[16] B. Vivacqua,[3] F. C. Volle,[54] D. vom Bruch,[13] N. Voropaev,[44] K. Vos,[81] C. Vrahas,[59] J. Wagner,[19] J. Walsh,[35] E. J. Walton,[1,57] G. Wan,[6] A. Wang,[7] B. Wang,[5] C. Wang,[22] G. Wang,[8] H. Wang,[73] J. Wang,[6] J. Wang,[5] J. Wang,[4,m] J. Wang,[74] M. Wang,[49] N. W. Wang,[7] R. Wang,[55] X. Wang,[8] X. Wang,[72] X. W. Wang,[62] Y. Wang,[75] Y. Wang,[6] Y. W. Wang,[73] Z. Wang,[14] Z. Wang,[4,m] Z. Wang,[30] J. A. Ward,[57] M. Waterlaat,[49] N. K. Watson,[54] D. Websdale,[62] Y. Wei,[6] J. Wendel,[83] B. D. C. Westhenry,[55] C. White,[56] M. Whitehead,[60] E. Whiter,[54] A. R. Wiederhold,[63] D. Wiedner,[19] M. A. Wiegertjes,[38] G. Wilkinson,[64,49] M. K. Wilkinson,[66] M. Williams,[65] M. J. Williams,[49] M. R. J. Williams,[59] R. Williams,[56] S. Williams,[55] Z. Williams,[55] F. F. Wilson,[58] M. Winn,[12] W. Wislicki,[42] M. Witek,[41] L. Witola,[19] T. Wolf,[22] G. Wormser,[14] S. A. Wotton,[56] H. Wu,[69] J. Wu,[8] X. Wu,[74] Y. Wu,[6,56] Z. Wu,[7] K. Wyllie,[49] S. Xian,[72] Z. Xiang,[5] Y. Xie,[8] T. X. Xing,[30] A. Xu,[35,v] L. Xu,[4,m] L. Xu,[4,m] M. Xu,[49] Z. Xu,[49] Z. Xu,[7] Z. Xu,[5] K. Yang,[62] X. Yang,[6] Y. Yang,[29] Z. Yang,[6] V. Yeroshenko,[14] H. Yeung,[63] H. Yin,[8] X. Yin,[7] C. Y. Yu,[6] J. Yu,[71] X. Yuan,[5] Y Yuan,[5,7] E. Zaffaroni,[50] M. Zavertyaev,[21] M. Zdybal,[41] F. Zenesini,[25] C. Zeng,[5,7] M. Zeng,[4,m] C. Zhang,[6] D. Zhang,[8] J. Zhang,[7] L. Zhang,[4,m] R. Zhang,[8] S. Zhang,[71] S. Zhang,[64] Y. Zhang,[6] Y. Z. Zhang,[4,m] Z. Zhang,[4,m] Y. Zhao,[22] A. Zhelezov,[22] S. Z. Zheng,[6] X. Z. Zheng,[4,m] Y. Zheng,[7] T. Zhou,[6] X. Zhou,[8] Y. Zhou,[7] V. Zhovkovska,[57] L. Z. Zhu,[7] X. Zhu,[4,m] X. Zhu,[8] Y. Zhu,[17] V. Zhukov,[17] J. Zhuo,[48] Q. Zou,[5,7] D. Zuliani,[33,h] and G. Zunica[50]

(LHCb Collaboration)

[1]*School of Physics and Astronomy, Monash University, Melbourne, Australia*
[2]*Centro Brasileiro de Pesquisas Físicas (CBPF), Rio de Janeiro, Brazil*
[3]*Universidade Federal do Rio de Janeiro (UFRJ), Rio de Janeiro, Brazil*
[4]*Department of Engineering Physics, Tsinghua University, Beijing, China*
[5]*Institute Of High Energy Physics (IHEP), Beijing, China*
[6]*School of Physics State Key Laboratory of Nuclear Physics and Technology, Peking University, Beijing, China*
[7]*University of Chinese Academy of Sciences, Beijing, China*
[8]*Institute of Particle Physics, Central China Normal University, Wuhan, Hubei, China*
[9]*Consejo Nacional de Rectores (CONARE), San Jose, Costa Rica*
[10]*Université Savoie Mont Blanc, CNRS, IN2P3-LAPP, Annecy, France*
[11]*Université Clermont Auvergne, CNRS/IN2P3, LPC, Clermont-Ferrand, France*
[12]*Université Paris-Saclay, Centre d'Etudes de Saclay (CEA), IRFU, Saclay, France, Gif-Sur-Yvette, France*
[13]*Aix Marseille Univ, CNRS/IN2P3, CPPM, Marseille, France*
[14]*Université Paris-Saclay, CNRS/IN2P3, IJCLab, Orsay, France*
[15]*Laboratoire Leprince-Ringuet, CNRS/IN2P3, Ecole Polytechnique, Institut Polytechnique de Paris, Palaiseau, France*
[16]*LPNHE, Sorbonne Université, Paris Diderot Sorbonne Paris Cité, CNRS/IN2P3, Paris, France*
[17]*I. Physikalisches Institut, RWTH Aachen University, Aachen, Germany*
[18]*Universität Bonn—Helmholtz-Institut für Strahlen und Kernphysik, Bonn, Germany*
[19]*Fakultät Physik, Technische Universität Dortmund, Dortmund, Germany*
[20]*Physikalisches Institut, Albert-Ludwigs-Universität Freiburg, Freiburg, Germany*
[21]*Max-Planck-Institut für Kernphysik (MPIK), Heidelberg, Germany*
[22]*Physikalisches Institut, Ruprecht-Karls-Universität Heidelberg, Heidelberg, Germany*
[23]*School of Physics, University College Dublin, Dublin, Ireland*
[24]*INFN Sezione di Bari, Bari, Italy*
[25]*INFN Sezione di Bologna, Bologna, Italy*
[26]*INFN Sezione di Ferrara, Ferrara, Italy*
[27]*INFN Sezione di Firenze, Firenze, Italy*
[28]*INFN Laboratori Nazionali di Frascati, Frascati, Italy*
[29]*INFN Sezione di Genova, Genova, Italy*
[30]*INFN Sezione di Milano, Milano, Italy*
[31]*INFN Sezione di Milano-Bicocca, Milano, Italy*
[32]*INFN Sezione di Cagliari, Monserrato, Italy*
[33]*INFN Sezione di Padova, Padova, Italy*
[34]*INFN Sezione di Perugia, Perugia, Italy*
[35]*INFN Sezione di Pisa, Pisa, Italy*
[36]*INFN Sezione di Roma La Sapienza, Roma, Italy*
[37]*INFN Sezione di Roma Tor Vergata, Roma, Italy*
[38]*Nikhef National Institute for Subatomic Physics, Amsterdam, Netherlands*
[39]*Nikhef National Institute for Subatomic Physics and VU University Amsterdam, Amsterdam, Netherlands*
[40]*AGH—University of Krakow, Faculty of Physics and Applied Computer Science, Kraków, Poland*
[41]*Henryk Niewodniczanski Institute of Nuclear Physics Polish Academy of Sciences, Kraków, Poland*
[42]*National Center for Nuclear Research (NCBJ), Warsaw, Poland*
[43]*Horia Hulubei National Institute of Physics and Nuclear Engineering, Bucharest-Magurele, Romania*
[44]*Authors affiliated with an institute formerly covered by a cooperation agreement with CERN*
[45]*ICCUB, Universitat de Barcelona, Barcelona, Spain*
[46]*La Salle, Universitat Ramon Llull, Barcelona, Spain*
[47]*Instituto Galego de Física de Altas Enerxías (IGFAE), Universidade de Santiago de Compostela, Santiago de Compostela, Spain*
[48]*Instituto de Fisica Corpuscular, Centro Mixto Universidad de Valencia—CSIC, Valencia, Spain*
[49]*European Organization for Nuclear Research (CERN), Geneva, Switzerland*
[50]*Institute of Physics, Ecole Polytechnique Fédérale de Lausanne (EPFL), Lausanne, Switzerland*
[51]*Physik-Institut, Universität Zürich, Zürich, Switzerland*
[52]*NSC Kharkiv Institute of Physics and Technology (NSC KIPT), Kharkiv, Ukraine*
[53]*Institute for Nuclear Research of the National Academy of Sciences (KINR), Kyiv, Ukraine*
[54]*School of Physics and Astronomy, University of Birmingham, Birmingham, United Kingdom*
[55]*H.H. Wills Physics Laboratory, University of Bristol, Bristol, United Kingdom*

[56]Cavendish Laboratory, University of Cambridge, Cambridge, United Kingdom
[57]Department of Physics, University of Warwick, Coventry, United Kingdom
[58]STFC Rutherford Appleton Laboratory, Didcot, United Kingdom
[59]School of Physics and Astronomy, University of Edinburgh, Edinburgh, United Kingdom
[60]School of Physics and Astronomy, University of Glasgow, Glasgow, United Kingdom
[61]Oliver Lodge Laboratory, University of Liverpool, Liverpool, United Kingdom
[62]Imperial College London, London, United Kingdom
[63]Department of Physics and Astronomy, University of Manchester, Manchester, United Kingdom
[64]Department of Physics, University of Oxford, Oxford, United Kingdom
[65]Massachusetts Institute of Technology, Cambridge, Massachusetts, USA
[66]University of Cincinnati, Cincinnati, Ohio, USA
[67]University of Maryland, College Park, Maryland, USA
[68]Los Alamos National Laboratory (LANL), Los Alamos, New Mexico, USA
[69]Syracuse University, Syracuse, New York, USA
[70]Pontifícia Universidade Católica do Rio de Janeiro (PUC-Rio), Rio de Janeiro, Brazil
(associated with Universidade Federal do Rio de Janeiro (UFRJ), Rio de Janeiro, Brazil)
[71]School of Physics and Electronics, Hunan University, Changsha City, China
(associated with Institute of Particle Physics, Central China Normal University, Wuhan, Hubei, China)
[72]Guangdong Provincial Key Laboratory of Nuclear Science, Guangdong-Hong Kong Joint Laboratory of Quantum Matter, Institute of Quantum Matter, South China Normal University, Guangzhou, China
(associated with Department of Engineering Physics, Tsinghua University, Beijing, China)
[73]Lanzhou University, Lanzhou, China
(associated with Institute Of High Energy Physics (IHEP), Beijing, China)
[74]School of Physics and Technology, Wuhan University, Wuhan, China
(associated with Department of Engineering Physics, Tsinghua University, Beijing, China)
[75]Henan Normal University, Xinxiang, China
(associated with Institute of Particle Physics, Central China Normal University, Wuhan, Hubei, China)
[76]Departamento de Fisica, Universidad Nacional de Colombia, Bogota, Colombia
(associated with LPNHE, Sorbonne Université, Paris Diderot Sorbonne Paris Cité, CNRS/IN2P3, Paris, France)
[77]Ruhr Universitaet Bochum, Fakultaet f. Physik und Astronomie, Bochum, Germany
(associated with Fakultät Physik, Technische Universität Dortmund, Dortmund, Germany)
[78]Eotvos Lorand University, Budapest, Hungary
(associated with European Organization for Nuclear Research (CERN), Geneva, Switzerland)
[79]Faculty of Physics, Vilnius University, Vilnius, Lithuania
(associated with Physikalisches Institut, Albert-Ludwigs-Universität Freiburg, Freiburg, Germany)
[80]Van Swinderen Institute, University of Groningen, Groningen, Netherlands
(associated with Nikhef National Institute for Subatomic Physics, Amsterdam, Netherlands)
[81]Universiteit Maastricht, Maastricht, Netherlands
(associated with Nikhef National Institute for Subatomic Physics, Amsterdam, Netherlands)
[82]Tadeusz Kosciuszko Cracow University of Technology, Cracow, Poland
(associated with Henryk Niewodniczanski Institute of Nuclear Physics Polish Academy of Sciences, Kraków, Poland)
[83]Universidade da Coruña, A Coruña, Spain
(associated with La Salle, Universitat Ramon Llull, Barcelona, Spain)
[84]Department of Physics and Astronomy, Uppsala University, Uppsala, Sweden
(associated with School of Physics and Astronomy, University of Glasgow, Glasgow, United Kingdom)
[85]Taras Schevchenko University of Kyiv, Faculty of Physics, Kyiv, Ukraine
(associated with Université Paris-Saclay, CNRS/IN2P3, IJCLab, Orsay, France)
[86]University of Michigan, Ann Arbor, Michigan, USA
(associated with Syracuse University, Syracuse, New York, USA)
[87]Ohio State University, Columbus, USA
(associated with Los Alamos National Laboratory (LANL), Los Alamos, New Mexico, USA)

[a]Deceased.
[b]Also at Lamarr Institute for Machine Learning and Artificial Intelligence, Dortmund, Germany.
[c]Also at Università degli Studi di Milano-Bicocca, Milano, Italy.
[d]Also at Università di Roma Tor Vergata, Roma, Italy.
[e]Also at Università di Modena e Reggio Emilia, Modena, Italy.
[f]Also at Department of Physics and Astronomy, University of Victoria, Victoria, Canada.

[g]Also at Università di Ferrara, Ferrara, Italy.
[h]Also at Università di Padova, Padova, Italy.
[i]Also at Facultad de Ciencias Fisicas, Madrid, Spain.
[j]Also at Università di Bologna, Bologna, Italy.
[k]Also at Università di Genova, Genova, Italy.
[l]Also at Università degli Studi di Milano, Milano, Italy.
[m]Also at Center for High Energy Physics, Tsinghua University, Beijing, China.
[n]Also at Universidad Nacional Autónoma de Honduras, Tegucigalpa, Honduras.
[o]Also at Università di Cagliari, Cagliari, Italy.
[p]Also at Centro Federal de Educacão Tecnológica Celso Suckow da Fonseca, Rio De Janeiro, Brazil.
[q]Also at Università di Bari, Bari, Italy.
[r]Also at Università di Perugia, Perugia, Italy.
[s]Also at LIP6, Sorbonne Université, Paris, France.
[t]Also at Università di Pisa, Pisa, Italy.
[u]Also at Hangzhou Institute for Advanced Study, UCAS, Hangzhou, China.
[v]Also at Scuola Normale Superiore, Pisa, Italy.
[w]Also at Università di Bergamo, Bergamo, Italy.
[x]Also at Universidad de Ingeniería y Tecnología (UTEC), Lima, Peru.
[y]Also at Università di Siena, Siena, Italy.
[z]Also at Università della Basilicata, Potenza, Italy.
[aa]Also at Universidad de Alcalá, Alcalá de Henares, Spain.
[bb]Also at Università di Urbino, Urbino, Italy.